Formation and evolution of field galaxies

JENS ANDERSSON

Department of Astronomy and Astrophysics
Centre for Astrophysics and Space Science
CHALMERS UNIVERSITY OF TECHNOLOGY
Göteborg, Sweden 2003

MASTER OF SCIENCE THESIS

Formation and evolution of field galaxies

JENS ANDERSSON

Department of Astronomy and Astrophysics
Centre for Astrophysics and Space Science
CHALMERS UNIVERSITY OF TECHNOLOGY
Göteborg, Sweden 2003

Formation and evolution of field galaxies
JENS ANDERSSON

Centre for Astrophysics and Space Science
Onsala Space Observatory
SE-439 92 Onsala
Sweden
Telephone: +46−(0)31−772 5500
jens@oso.chalmers.se

Chalmers Reproservice
Chalmers Tekniska Högskola
Göteborg, Sweden 2003

Formation and evolution of field galaxies

JENS ANDERSSON
Department of Astronomy and Astrophysics
Centre for Astrophysics and Space Science
Chalmers University of Technology

Abstract

The main goal of this Master's thesis was to study the field galaxy population in order to understand how galaxies form and evolve.

The data used is from ESO Imaging Survey, Deep Public Survey and consist of broad band optical and infrared (UBVRIJK$_s$) observations of Chandra Deep Field South (CDF-S). Source detection and photometry was performed using SExtractor. Photometric redshifts for 21 053 galaxies were obtained using a template-fitting technique with a bayesian prior. The rms dispersion of the redshifts were found to be 0.13(1+z) in the redshift range $0.2 < z < 2.3$, when comparing with spectroscopic redshifts. Completeness corrected number counts of galaxies have been produced. A comparison of the observed counts with models show that a simple luminosity evolution model fail to reproduce the observed counts at intermediate magnitudes while a non-evolution model fail to fit the observations at faint magnitudes. Evolution of the rest-frame colour distributions of the galaxies has been studied by binning the galaxies in redshift intervals. It is found that inherently "red" galaxies gets reddened by 0.5 magnitudes over the redshift interval 0.3-1.3. The relative numbers of bright blue galaxies are found to increase with redshift up to $z \sim 1.5$. Evolution of spectral types with redshift is also studied, the main conclusion is that late type galaxies are much more common at high redshift than at low.

Keywords: galaxies:evolution – galaxies:photometry – cosmology:observations

Preface

This master's thesis for a degree in Engineering physics was carried out at Onsala Space Observatory and partly at Space Telescope Science Institute (STScI). These two places conveniently summarizes all the things that I like about working with astronomy. The nice and very open atmosphere at Onsala was really great to work in, there were always people to talk to when the problems got too big. At STScI I was really excited to meet the very same people, whose work I had read and tried to understand during the first part of the year. It was also very interesting to attend some of the huge amount of the seminars that were offered at STScI.

During the year I spent working with this project, I have come to realise that doing research in astrophysics is not always about finding new exciting results and looking at newly obtained data. It is about working hard and trying to solve problems that keep popping up, even for tasks that might have seemed simple in the beginning. It is also about finding new ways to study very old phenomena and discussing things both big and small with your collegues. It is about standing in the dark and enjoying a perfect starry sky, but also about yelling at the computer when it crashes for the tenth time in one single day. But most of all it is about finding out how things work.

Acknowledgements

First and foremost I would like to thank my supervisor **Duília de Mello** for making this project possible. The encouragement and advice she gave me, and the numerous discussions we had, during this year were the most important contributions to this thesis.

I thank the people at Onsala Space Observatory for making me feel welcome and for all interesting conversations at the coffe breaks (covering everything from nobel prize physics to strange paintings of Napoleon). A special thanks goes to my fellow master's students, **Theresa Wiegert**, **Eva Karlsson**, **Evert Olsson** and **Rodrigo Parra** for all the good times we had. I am also grateful to **Stefan Bergström** for helping me solve the problems I had with matching catalogues and for providing me with the nice thesis template. I would also like to thank all the people I met at Space Telescope Science Institute in Baltimore for helping me feel at home despite snow storms, and a long way home. I am grateful to **Thomas Dahlén** for helping me understand the photometric redshift methods. A heartfelt thanks goes to **Peter Weilbacher** at University of Durham for invaluable help with the number count models.

Thanks to my friends and family for supporting me and giving me something else to think about when the problems of the project seemed to be unsolvable. Finally I thank **Moa** for always being by my side.

This research project has made use of data from the ESO Imaging Survey, Deep Public Survey. Observations have been carried out using the MPG/ESO 2.2m Telescope and the ESO New Technology Telescope (NTT) at the La Silla observatory under Program-ID No. 164.O-0561.

Contents

1

Introduction

Observational studies of galaxy evolution and formation has for a long time been impossible. The dual problem of observing galaxies very far away is that a very deep (i.e. going for the faintest objects) survey must be combined with a large field of view. If a small volume is studied, how can we then know that the detected objects and their properties are representative of the universal population of galaxies? The CCD technique has made this possible, by combining large mosaics of photo-sensitive cells with the large dynamic range (which make it possible to detect the faintest objects without saturating the instrument on the brighter objects) of modern CCD's. The large ground based telescopes that has been built during the latest decade (e.g. VLT, Keck) have made it possible to get deep enough using reasonable exposure times. One of the first, and probably most important, really deep surveys is the HDF-N (Hubble Deep Field-North) taken with the Hubble space telescope (Williams et al. 1996). These observations made the distant universe come to life, in the high resolution images galaxies of all types can be seen. Groups of interacting spiral galaxies as well as elliptical loners stand out as beacons in an area of the sky where nothing had been seen before. This revolution in astronomical instrumentation is clearly visible when counting the amount of papers published on galaxy evolution (Ellis 2001).

The fact that the speed of light is finite means that distant galaxies are also far away in time. The photons detected at earth has traveled for billions of years before ending their existences in the astronomer's eye. This means that if the distance to the galaxy can be correctly determined, the time when the galaxy sent out that light is also known. All galaxies (that are sufficiently far away) are receding away from us, this is the most clear evidence we have for the expansion of the universe. The light from distant galaxies is thus *redshifted* and astronomers use redshift (z) as a measure of the distance to the objects, but also as an indicator of the so called *look-back time* (i.e. how long ago the light from the galaxy was

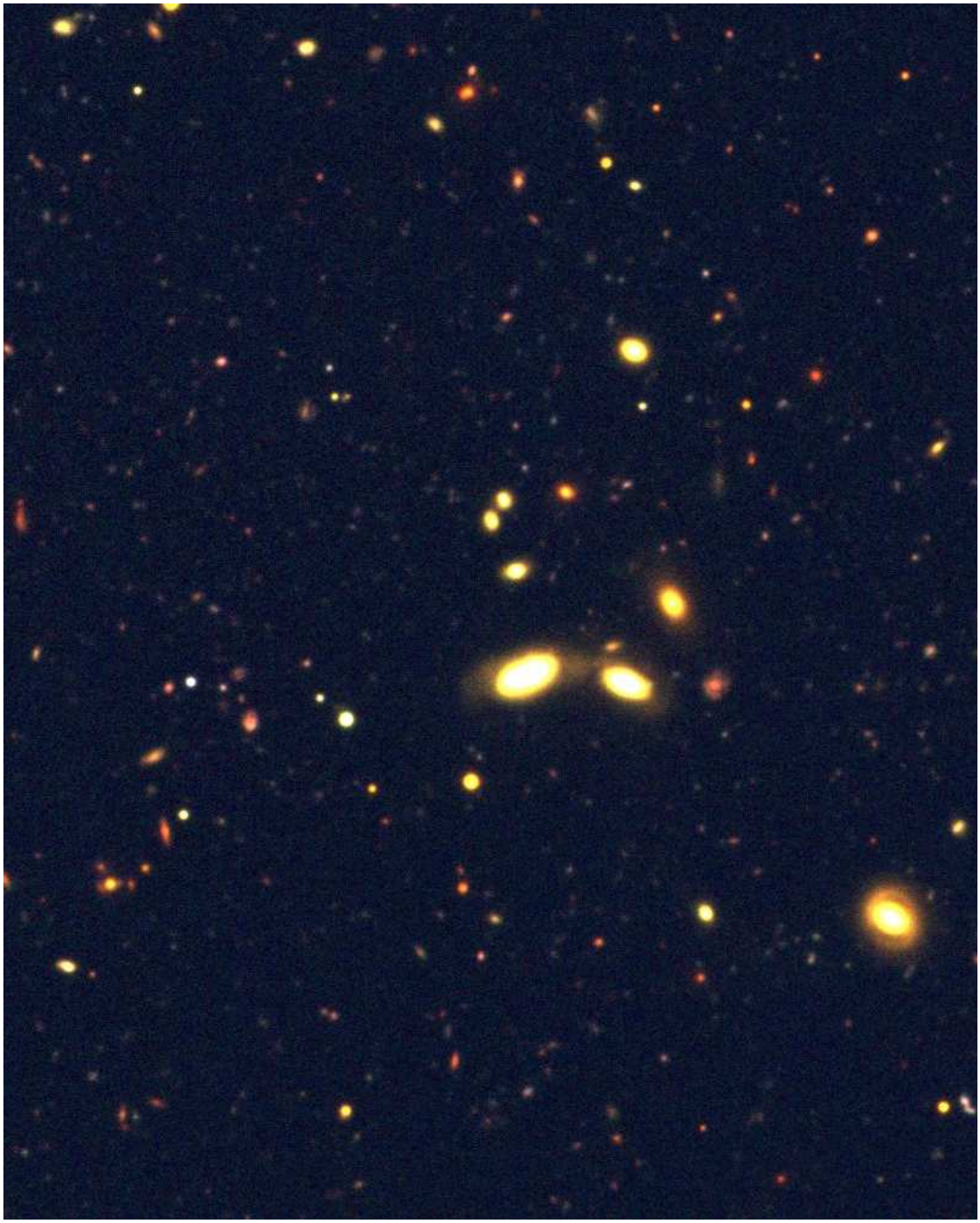

Figure 1.1: Colour composite image showing a small part of the Chandra Deep field South (CDF-S). Three images (from ESO's Deep Public Survey) obtained with different filters have been used.

radiated). So in order to study the evolution of galaxies we need to measure their redshifts. For large surveys where a large number of faint galaxies are studied it becomes next to impossible to obtain spectroscopic redshifts (i.e. finding the shift in a spectrum of the object) for all of the objects. Instead, photometric redshift techniques have been developed to estimate redshifts (e.g. Connolly et al. 1995; Gwyn 1995; Fernández-Soto, Lanzetta & Yahil 1999; Benítez 2000). Using these techniques redshifts for thousands of galaxies have been found.

One of the first tools of observational cosmology is the number counts of galaxies. Cosmological theories predict how many galaxies we should see in a limited area of the sky, and how galaxies should be distributed in luminosity. With larger and larger surveys being undertaken, the observational errors in the galaxy counts are getting smaller and smaller. Already the very first studies of number counts (e.g. Shanks et al. 1984 see also Kron 1980) could establish that the universe was in fact non-Euclidean. Nowadays the data from large surveys of both local (e.g. SDSS, Yasuda et al. 2001) and high redshift galaxies (e.g. HDF-N and S, Postman et al. 1998; Metcalfe et al. 2001) are used to investigate cosmological parameters and galaxy evolution. The data from observations are compared to counts from models of galaxy formation and evolution (e.g. Campos 1995; Nakata et al. 1999; Nagashima et al. 2002). In this thesis observations from a large survey have been used to construct normalized galaxy counts, which are then compared to different models.

There is of course more to galaxies than what meets the eye (i.e. how many photons that meet the eye). Apart from their luminosities, galaxies also have other important properties. The colour of a galaxy can, for example, tell us whether it is still forming stars or not. The shape (or morphology) of the galaxy is also an interesting property which is also correlated to many other properties. Several authors have studied the colour distribution of local galaxies (e.g. Hogg et al. 2002), others have investigated how the colours of galaxies evolve with redshift (Lilly et al. 1995b; Im et al. 2002; Ellis 2001). The colour evolution of galaxies can give us important clues to how star formation is turned on and off. Information on the morphology of galaxies (for high redshift galaxies space-based high-resolution imaging is needed to resolve the different parts in a galaxy) have been used to find out how the different galaxy types evolve and how they correlate with the colour distributions (Abraham et al. 1996). In this thesis I investigate the colour evolution of galaxies and the galaxy type (based on spectral type, which is concept described later) distributions at different redshift intervals.

Chapter 2 is devoted to basic astrophysical theory. It contains definitions and equations used in this work. A short introduction to how survey data can be analyzed and what conclusions can be drawn from the data are also given. Finally the current theories of galaxy formation and evolution are described. The knowledgeable reader can safely skip this chapter and move on to the next chapter.

Chapter 3 contains a description of the data set used, the basic properties of the data, the detection method and the photometry performed. The photometric

redshifts obtained for the detected galaxies and different methods are discussed. Rest-frame magnitudes are also computed. Thereafter the main results are presented, beginning in chapter 4 with the completeness-corrected number counts of galaxies in the observed field. The counts are also compared to simulations. In chapter 5 the evolution of galaxies is investigated by studying the rest-frame colours of the galaxy population binned in redshifts. This chapter ends with a study of the spectral type distribution of galaxies in different redshift intervals. In chapter 6 the conclusions of the work are given together with an outlook section which describes possible future work to be done using the data.

In this work I have assumed a flat λ-dominated cosmology (i.e. λCDM) with $\Omega_\lambda = 0.7$, $\Omega_M = 0.3$ and a Hubble constant $\mathrm{H}_0 = 70$ km s^{-1} Mpc^{-1}.

2

Background and Theory

2.1 Basic astrophysical theory

2.1.1 Luminosities, magnitudes and filters

The origin of the techniques astronomers use to measure the brightness of objects in the sky can be traced back to ancient Greece (120 B.C.), when the greek philosopher Hipparcos classified stars visible to the naked eye by *magnitudes*. The brightest stars were put into the first magnitude class, the stars were then classified uniformly in magnitudes by their brightness as seen by the naked eye. The faintest stars were put in the sixth class. Ptolemy later put this into the first known stellar catalogue, the *Almagest*, this scale was used for more than 2000 years and influenced the modern astronomy to use the magnitude system of measuring luminosities (Sterken & Manfroid 1992).

Since the human eye perceives light logarithmically this corresponds to a logarithmic relation between the radiation flux (called luminosity by astronomers) and magnitude. In modern astronomy this has been formalized, the so called *apparent* magnitude of objects is related to its luminosity by the relation,

$$m = -2.5\ log(F) + m_{zp}, \tag{2.1}$$

where F is the flux observed by the instruments and m_{zp} is the magnitude zero-point which is found by calibrating the measurements against some source with known magnitude. The *absolute* magnitude of objects is defined as the apparent magnitude an object would have if it were at a distance of 10 parsecs (1 parsec $= 3.086 \times 10^{16} m = 3.26$ light years), quite nearby in astronomical terms. The flux is inversely proportional to the square of the distance, so the absolute magnitude can be written;

$$M = m + 5 - 5\ log\ r, \tag{2.2}$$

with the distance r in parsecs. The absolute magnitude gives an estimate of an object's intrinsic brightness. In general, equation 2.2 is more complicated, the chosen filter set will add a term and for very distant objects even space-time itself will start to affect the equation (the dependence on r will be different due to cosmology corrections), more details on this is given in chapter 2.4.

There is also a wavelength dependence hidden in the magnitude definitions. The naked eye magnitudes used by astronomers until the arrival of photography, is in reality not a measurement of the entire flux from an object. The human eye acts as a photometric filter, picking up photons with energy corresponding to wavelengths between $\sim$ 400 nm (blue) and $\sim$ 800 nm (red). The expression for the magnitude (equation 2.1) in reality becomes:

$$m_f = -2.5\ log \int_{\lambda_1}^{\lambda_2} F(\lambda) S_f(\lambda) d\lambda + m_{zp}, \tag{2.3}$$

where λ_1 and λ_2 are the lower and upper wavelength limits of the filter and $S_f(\lambda)$ is the sensitivity curve of the filter (f) under consideration. This equation also describes the wavelength dependence of any filter used in artificial photometry.

Modern astronomy uses charge-coupled devices (CCD's) instead of photographic plates to detect photons. In a CCD many pixels (for example 1 024 $\times$ 1 024 pixels) form a *mosaic* of small photodetectors. To study colours of the objects, magnitudes in different wavelength *bands* is measured by introducing a filter before detection in the CCD. The sensitivity of some commonly used filters is shown in figure 2.1. In general, filters used in various instruments are not exactly the same. This means that in order to compare the magnitudes of different measurements it is necessary to correct the magnitudes to the same filter system. The process of transforming the magnitudes into a specific filter system is called *color correction*. For an excellent discussion on magnitudes and different filter systems see Sterken & Manfroid (1992). A traditional filter system, which has been in use for many years is the Johnson-Morgan-Cousin system. The magnitudes in the different filters are given capital letters (central wavelength in parenthesis); U (365 nm), B (440 nm), V (550 nm), R (720 nm), I (900 nm). It has also been extended to the infrared, J (1.25 μm) and K_s (2.2 μm). The system is then finally defined by choosing a magnitude zeropoint. The zeropoint is fixed by stating that the star Vega (α Lyrae) has zero magnitude in all filters. Later on this was revised so that a standard A0 star would have zero magnitude in all filters, and a mean calibration has since then been established. The colours of objects are thus related to the colour of Vega (i.e. a star which has the same colour as Vega has zero colour).

For large surveys of tens of thousands of objects, it is important that the data can be combined easily without performing additional filter transformations. Instead of a filter system that puts a measured star (or a mean of many stars) as zeropoint, the AB filter system uses a constant m_{zp} for all filters (Oke & Gunn

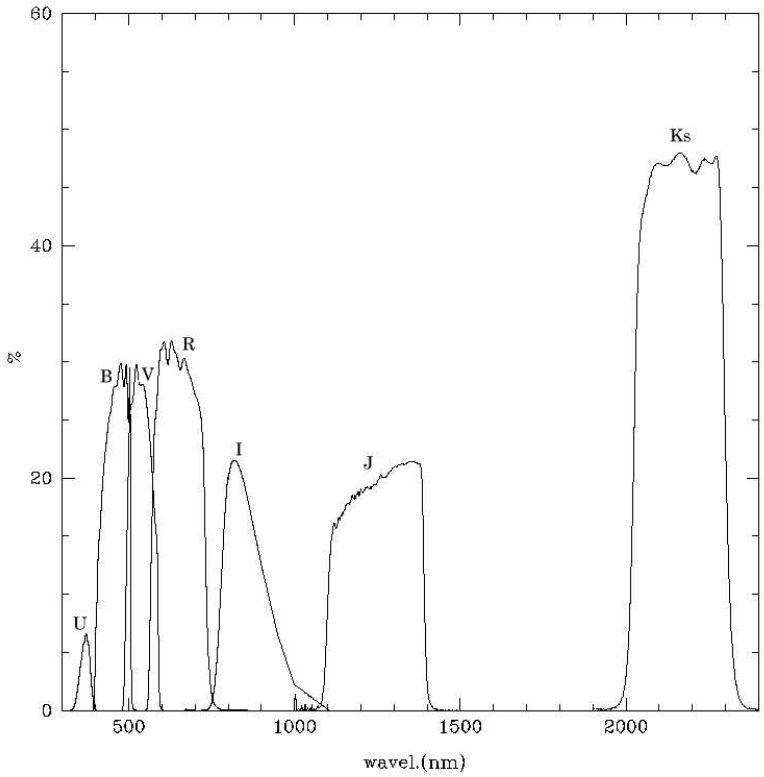

Figure 2.1: Transmission (sensitivity, $S_f(\lambda)$) curves of filters UBVRIJK$_s$ (WFI and SOFI, see chapter 3.1). The apparent magnitudes in the different filters covers different parts of the spectrum.

1983). AB magnitudes are normally denoted U_{AB}, V_{AB} and so on. The constant m_{zp} is set so that $V_{AB} = V$, and the definition becomes:

$$m_{AB} = -2.5\ log(F)\ - 48.60. \tag{2.4}$$

The AB magnitude system has the property that an object with a flat spectrum, i.e. with constant flux per unit frequency interval, has zero colour. This makes it very suitable for studying colours of objects.

2.1.2 An expanding universe, redshifted galaxies

The fact that almost all galaxies in the sky seems to be moving away from us, led astronomers and cosmologists to the conclusion that the universe is in fact expanding. The light emitted from receding galaxies experience a relativistic Doppler shift, the galaxies are said to be *redshifted*. The wavelength of the radiation is lengthened and thus shifted to the red part of the spectrum. The redshift z of a galaxy

is defined in terms of the rest-frame wavelength, λ_0 and the observed wavelength, λ;

$$1 + z = \frac{\lambda}{\lambda_0}. \tag{2.5}$$

For small z the velocity, v, is related to the distance to the galaxy through Hubble's law, $v = H_0 D$, where D is the distance and H_0 the *Hubble constant*, which also is a measure of the expansion velocity at the current epoch. For larger redshifts the relation is more complicated (see chapter 2.4). The Hubble constant, together with the density of the universe, are the cosmological parameters that can be used to make cosmological corrections on the observations. The density of the universe is expressed as the dimensionless parameter Ω which is equal to 1 for a flat (in the space-time sense) universe.

The important aspect to remember about redshifts is that since the light travel at finite velocity the more distant galaxies (with higher z) are in fact also young galaxies, i.e. the overall galaxy population is younger for higher redshifts. This means that if we want to study the evolution of galaxies, we can compare the properties of galaxies at different z.

2.2 Source detection and photometry

Modern instruments used in astronomy produce images which are recorded in the so called FITS-format, this is the output of CCD cameras. An image is basically a large table with one entry (flux value) for each pixel. The observed raw data is first reduced to science frames by running it through a number of steps. Among those steps are flat-fielding (correcting for sensitivity variations across the pixel mosaic), astrometric calibration (i.e. finding the correct sky coordinates in the image) and the determination of a magnitude zero point. In the data reduction process weight images can also be produced, these images can be used to weight different parts of the CCD mosaic differently. This becomes especially important when dealing with composed images, where many CCD images have been joined to form a mosaic. It is important to remember that for ground-based observations the resolution is rarely limited by the instrument. Instead it is the atmospheric conditions which limit the resolution, this is called *seeing*. The seeing causes point sources (like stars) to become "smeared out", so instead of one pixel the star might fill several. The resolution of an astronomical image is generally quantified by the FWHM of the point spread function (PSF) measured on the frame. For ground-based images this is caused by seeing, but for space-based observations the PSF is instead tied to the instrument used.

The fully reduced science and weight frames is the final outcome from the observations. The resulting images can be analyzed, the brightness of sources on the images can be measured using a variety of programs. For large surveys the amount of sources in one image can be of the order 10^5, this means that the

detection of sources in the image cannot be done by eye. Instead a code is used to produce source catalogs. If the targeted type of objects are faint galaxies (or stars) *masking* must also be done on the image. The brightest sources (in most cases these are stars) saturate the CCD and causes flux to overflow into adjacent pixels. Areas close to bright stars in the image will generally be severely affected by this and the solution is to mask out these areas (i.e. setting their flux to zero). A typical masked image can be seen in figure 3.1.

2.2.1 Source detection with SExtractor

The most widely used source detection program is SExtractor (Bertin & Arnouts 1996). The detection algorithm performed by SExtractor (hereafter SE) goes through a number of steps before yielding the final catalogues. The first step computes the background (noise) level in the image; a poor resolution background map is produced which is then subtracted from the original image. If wanted, a weight image can also be used in this step. Each pixel in the image is then given a weight by combining and normalizing the science and weight frames. The second step is to smooth the image by convolving the image with a Gaussian (or other types of functions) with a FWHM roughly the same size as the PSF of the image. This process decreases the noise level in the image by a factor ~ 10, which of course makes detection more effective (Bertin & Arnouts 1996).

In the parameter file for the program a *detection threshold* is set. This threshold tells SE which pixels it should consider to be detected. Another parameter that affects the detection directly as well is the minimum number of connected pixels which are all above the detection threshold. This yields a number of possible sources, which are then further analyzed. Objects that are very close to each other might be considered a single object after this basic detection. Each object is therefore checked to see if they have a "dip" in the radial luminosity profile. In this way, for example merging galaxies can be separated.

The source catalogue is also cleaned for spurious objects. The cleaning algorithm only finds the most obvious false sources. It checks for saturation in the CCD close to very bright objects and also for so called optical "ghosts" (Bertin & Arnouts 1996). The end result is a catalogue of sources and their positions in pixels (image scale) and sky coordinates (assuming the data contain coordinate information). SE can also perform photometry on the detected sources, either aperture magnitudes (measure the flux in an aperture with constant size) or total magnitudes which can be estimated in various ways. The photometry can be done on the unconvolved original images or on the detection images. A magnitude error based on the noise level around each object is also calculated.

To quantify the depth (i.e. how faint can objects be detected) of the observations, one uses the concept of a limiting magnitude, which is the faintest magnitudes for which objects can be detected. This is related to the noise level; e.g. Arnouts et al. (1999) finds that their R band 5σ limiting magnitude is 25.5. This means that

sources brighter than $R = 25.5$ should have errors less than 0.2 magnitudes. To find this I assume that the σ level is the same as the signal to noise ratio, S/N, and that the magnitude errors are given by the inverse of S/N ratios (valid for small errors, see Sterken & Manfroid 1992). To find an approximate limiting magnitude I define an aperture (normally 2× FWHM of the PSF measured on the frame). Then the magnitude in such an aperture is computed using the noise level (rms) of the image (which is also measured by SE). The 5σ limiting magnitude is thus given by:

$$m_{5\sigma lim} = m_{zp} - 2.5\ log_{10}\left(5 \times rms \times \sqrt{\frac{\pi D^2}{4\Theta^2}}\right), \tag{2.6}$$

D is the aperture diameter in arcseconds and Θ is the resolution in arcseconds per pixel.

To separate galaxies and stars SE also provides an artificial neural network algorithm which give each object a value between 0 and 1 (the CLASS_STAR value), where 1 is almost certainly a star and 0 a galaxy. The most important property of the object when determining the CLASS_STAR value is the FWHM of the radial luminosity profile. If this is very close to the PSF of the frame then the object is a point source and therefore probably a star (but could of course be any kind of point source, like a quasar). The classification algorithm breaks down at faint magnitudes, but for faint magnitudes in the R or I band one would expect few stars anyway.

2.2.2 Completeness

When investigating populations of galaxies of a certain luminosity it becomes important to know whether the source catalogues really contain **all** galaxies in the given luminosity range. For very faint galaxies, close to the limiting magnitude, we can be certain that some galaxies have not been detected. The limiting magnitude is in reality not a fixed limit, but a more continuous "fade-out" of detections. At the 1σ limit the percentage of detected galaxies can be as low as 10 %. The reasons for incompleteness vary but the most important one is that because galaxies come in different shapes and types, some of them are easier to detect than others. One group is particularly hard to detect, these are the *low surface brightness (LSB) galaxies*, which have a very low luminosity per pixel but might have a fairly bright total luminosity due to their large sizes. So as we go fainter and fainter these galaxies will not be detected despite the fact that their total luminosities are higher than the limiting magnitude. This is of course also affected by the adopted detection algorithm, some algorithms might find the LSB galaxies more easily.

Another factor that determines the completeness levels is how effective the detection software separates galaxies which are very near to each other. The faintest magnitudes objects are generally harder to separate because the noise blurs the

flux peaks, so two objects might be detected as one and thereby reducing the completeness. If the source detection program used contains a star-galaxy separation algorithm we will also get incompleteness due to the misclassification of galaxies as stars. This can be investigated by using, for example, the colour distribution of objects. For a discussion on how to correct for the incompleteness see chapter 3.2.

2.3 Photometric redshifts

The redshift of galaxies is normally determined by matching the observed spectral lines to their rest-frame counterparts. In this way very accurate redshift measurements can be made. But it takes much longer time to obtain the spectrum of a galaxy than just the image. This is because spectrography is in general much less sensitive than photometry, since the measured flux is integrated over a much smaller wavelength range to obtain good wavelength resolution. For faint galaxies it becomes next to impossible to obtain spectra. The process of obtaining spectroscopic redshifts is thus quite time-consuming and for surveys which can include up to 100 000 galaxies with the faintest ones the most numerous, another approach is needed. The solution is to use a so called photometric redshift technique. With this technique photometry in a number of broad band filters (e.g. UBVRI) is used to find the redshift of the galaxy. The two main photometric redshift methods are the empirical training set method and the template fitting or spectral energy distribution (SED) fitting method. In general, both methods aim to find the function $z(C_n)$, i.e. the redshift given by the colours of the galaxy.

2.3.1 The empirical training set method

The empirical training set method (e.g. Connolly et al. 1995) tries to establish a continuous relation by using galaxies for which a spectroscopic redshift has been determined, then the colours of galaxies with unknown redshift can be mapped onto the relation and the redshifts found. One of the problems with this method is that for fainter galaxies and a large redshift range the function $z(C_n)$ becomes degenerate, the colours of a galaxy might be the same for different z. Another problem is that spectroscopic redshifts are needed to construct the $z(C_n)$ relation, for redshifts $\gtrsim 1$ most galaxies start to become too faint for spectrographs and it becomes hard to construct a valid relation (Benítez 2000).

2.3.2 The SED fitting method

The SED-fitting method instead uses a library of spectral energy distributions that are redshifted to produce the inverted relation $C_T(z_T)$, where the T is the spectral type. The colours are then matched to the observed colours and the the best-fitting (in a maximum likelihood, ML, sense) redshift is chosen to be the correct one. For

a pure ML method the best fit is given by the minimum χ^2 with respect to redshift and galaxy type;

$$\chi^2(T, z, m_\alpha) = \sum_i \frac{(m_{obs;i} - (m_{t;i}(T, z) + m_\alpha))^2}{\sigma_i^2}, \tag{2.7}$$

where i denotes the filter, the sum goes through all the available filters. The magnitudes, m_{obs} and m_t, are the observed and template magnitudes respectively and σ is the uncertainty in observed magnitude. The template normalization factor m_α is also needed to fit the template magnitudes to the observed apparent magnitudes (Dahlén, Fransson & Näslund 2002). Figure 2.2 illustrates the template fitting.

For an excellent discussion on the similarities and differences of the two methods see Benítez (2000). Since I would like to study the galaxy population for $z \gtrsim 1$, I chose to use a SED-fitting method. Several authors have used SED-fitting methods to find photometric redshifts (e.g. Gwyn 1995; Fernández-Soto, Lanzetta & Yahil 1999; Bolzonella, Mirales & Pelló 2000; Benítez 2000; Dahlén, Fransson & Näslund 2002) some of them have made their codes publicly available. I have used two of the public codes, HyperZ (Bolzonella, Mirales & Pelló 2000) and BPZ (Benítez 2000). HyperZ is basically a ML method but with more free parameters, instead of using the empirically obtained templates of Coleman, Weedman &Wu (1980) they use synthetic SED's. By using synthetic SED's they can also include the age of galaxies and the internal extinction (reddening) of the galaxies as free parameters. It provides good redshift estimates if the photometry is good, but suffers quite a lot of *template mismatching*, i.e. the galaxy is assigned to the wrong galaxy type. This causes the rate of "catastrophic" redshifts (where I define catastrophic redshifts to be objects with $|z_{phot} - z_{spec}| > 1$) to be quite high ($\sim 10 - 20$ % for my data set).

2.3.3 Bayesian redshift estimation

The publicly available program BPZ (Benítez 2000) is basically a SED-fitting photometric redshift method, but with the addition of a bayesian magnitude prior to the maximum likelihood analysis. By using a prior the number of catastrophic redshift estimations can be lowered. Six different templates are used, four from Coleman, Weedman &Wu (1980); E, Sbc, Scd and Im, and two starburst templates from Kinney et al. (1996) (see figure 2.3). To obtain the template magnitudes in the broad bands the filter transmission functions are convolved with the redshifted spectral energy distributions (SEDs) of the six templates. The templates are also corrected for Madau damping, i.e. correcting for internal absorption in the galaxies (Madau 1995). By using a prior the number of catastrophic redshift estimations can be lowered.

The task of finding the photometric redshifts with a bayesian probability method can be formulated as finding the redshift for which the probability $p(z|D, I)$ has a maximum. This is the probability that a galaxy will have redshift z given the data

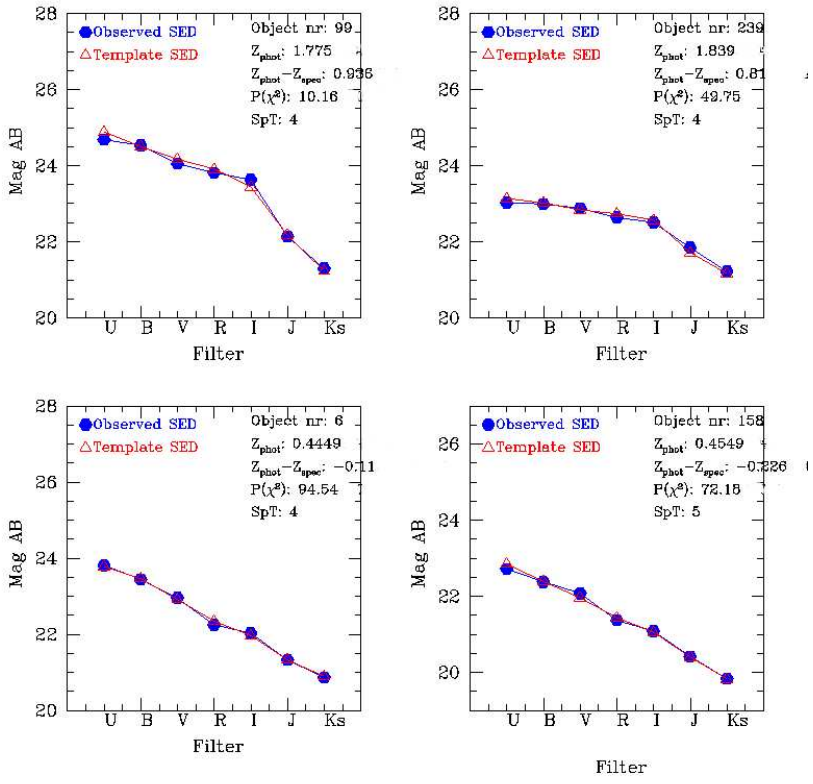

Figure 2.2: The observed and the best-fit template SED's, for a selection of objects. As can be seen the large differences in the SED fit yields error in the photometric redshifts. These fits have been obtained using HyperZ (Bolzonella, Mirales & Pelló 2000), a ML method.

$D = \{C_n, m_0\}$ (where C_n are the colours used and m_0 is the magnitude used for the prior) and the prior information I. But this does not take the different spectral types into account, so the probability is expanded into the basis $p(z, T|D, I)$ (which is the probability that a galaxy has both redshift z and spectral type T). The total probability is given by the sum of these,

$$\begin{aligned} p(z|C_n, m_0, I) &= \sum_T p(z, T|C_n, m_0, I) \\ &\propto \sum_T p(z, T|m_0, I) p(C_n|z, T), \end{aligned} \tag{2.8}$$

Bayes' theorem is applied to get the proportionality. On the left hand side $p(C_n|z, T)$ is the probability that we observe colours C_n given a redshift z and a galaxy type T. This probability is obtained by fitting the template magnitudes to the observed magnitudes. The other factor on the left hand side is the prior probability,

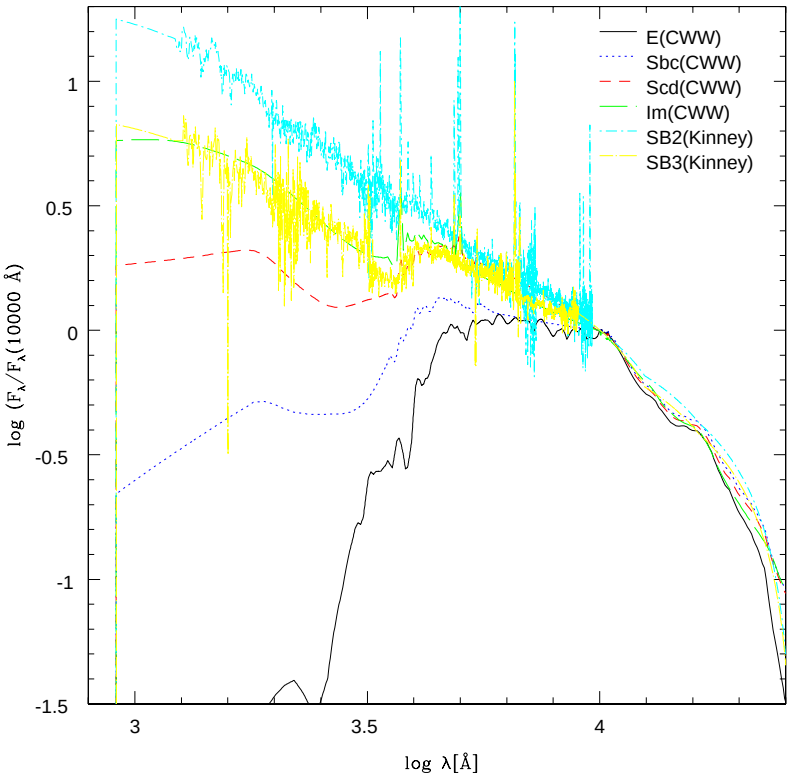

Figure 2.3: Spectral energy distributions of the six galaxy types used in the photometric redshift estimation. They are all normalized at 10000 Å. E, Sbc, Scd and Im templates from Coleman, Weedman &Wu (1980), SB2 and SB3 from Kinney et al. (1996).

$p(z, T|m_0, I)$ which can be written as,

$$p(z, T|m_0, I) = p(T|m_0, I)p(z|T, m_0, I), \tag{2.9}$$

where the product rule was used. The first factor in the resulting expression is the probability of having a certain galaxy type for a given magnitude, the second is the probability that a galaxy has a certain redshift for a given type and magnitude. The I in the equation marks the use of prior information to compute these probabilities.

The use of a prior is what makes the bayesian method different from a normal ML method. In a ML method the found redshift is the one with the highest $p(C|z, T)$ irrespective of how probable the found combination of z and T is. Bayesian probability weights the likelihoods by the prior probabilities $p(z, T|m_0)$, thereby smoothing the probabilities and lowering the spurious probability peaks caused by noise (see figure 2.4). In the expression for χ^2 (equation 2.7) the prior information also enters in the template normalization factor. It gives rise to an

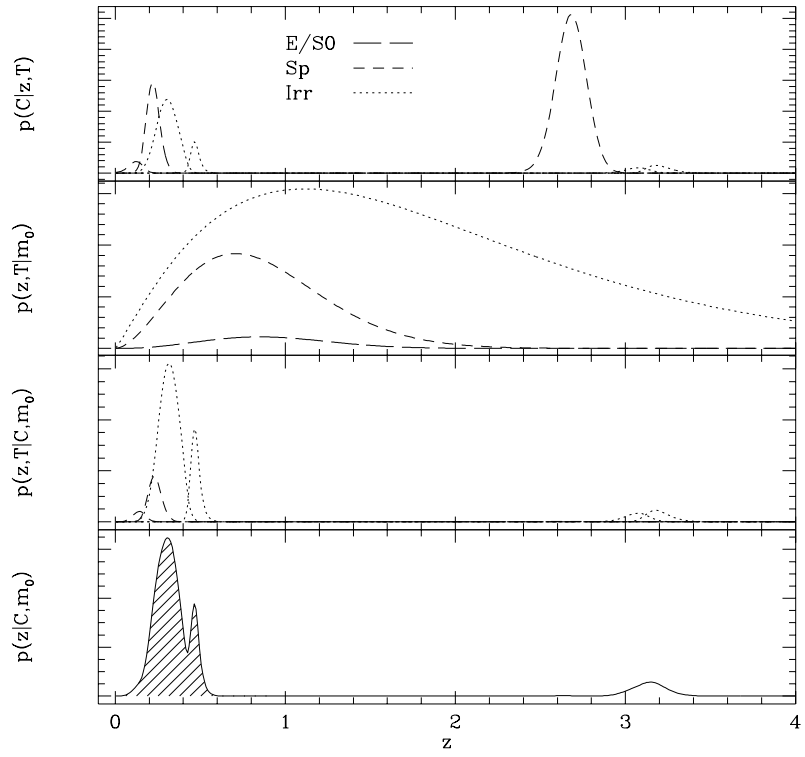

Figure 2.4: This plot shows the probability distributions in BPZ for a galaxy at z = 0.28 with Irr SpT and I $\simeq$ 26. From top to bottom we have 1) Probability distributions for a galaxy with given colours to be of a certain type and at a certain redshift. 2) The prior probability, i.e. the probability that a galaxy with a certain apparent magnitude will be at a certain redshift and of a certain type. 3) The resulting probability distribution using the prior for the different spectral types. 4) The final distribution for the most probable SpT. This figure is from Benítez (2000).

additional factor in the expression for the probability, Benítez (2000) show that the probability can be written:

$$p(C|z,T) \propto F(z)^{-1/2} exp\left[\frac{-\chi^2(T,z,\alpha)}{2}\right], \tag{2.10}$$

where F(z) is the additional factor.

When using a bayesian prior photometric redshift method there are some caveats that need to be considered. The prior used might bias the estimation of redshifts and introduce spurious effects (Bolzonella, Mirales & Pelló 2000). The prior used correspond to a given redshift and galaxy type distribution, and might thus bias

the estimation towards the prior. But one must also be aware that even when using a flat prior (which is the case in pure ML methods) a bias is introduced. The flat prior itself corresponds to an assumed distribution, but this distribution is easily found to be unphysical (Benítez, priv. comm.). The prior information is combined with the other data to form the entire probability distribution, it does not affect the redshift estimation strongly, except in cases when an ML method would have yielded a low probability redshift galaxy type combination.

2.4 Rest-frame magnitudes and colours

To find out the inherent properties of stars and galaxies the apparent magnitudes need to be converted into absolute magnitudes (see chapter 2.1.1). Since this means to convert the magnitudes into what they would have been if the observed galaxy was at rest (or placed at a distance of 10 parsecs from the Sun), the obtained magnitudes are called rest-frame magnitudes. In general a galaxy which is inherently "red" (i.e. brighter in the longer wavelengths than in the short) is older than a "bluer" galaxy (more on this in chapter 2.5). So if the inherent colours of a galaxy can be found, the age and composition of the galaxy might be determined. The conversion into rest-frame magnitudes contain two parts, the distance modulus effect and the K-correction effect. With m as the apparent and M as the absolute magnitude;

$$m = M + DM(z) + K(z, F, SpT), \tag{2.11}$$

DM is of course the distance modulus which is dependent on the redshift and K is the K correction factor which depends on the filter used (F), redshift of the galaxy and galaxy type (SpT).

2.4.1 Distance modulus

The distance modulus accounts for the distance dimming of a source that is far away. The total flux, F, from a source is radiated in all directions causing the flux density at a distance D from the source to be (this is bolometric luminosity for a arbitrary filter):

$$S = \frac{F}{4\pi D^2}, \tag{2.12}$$

this relation is valid for low redshift object, where cosmological effects have not yet become important. For the general case, the distance D is dependent on z, $D = D(z)$ (since the expansion of the universe affects the distances). However, there is also another more subtle effect that changes equation 2.12. Due to the fact that the universe is expanding, it was smaller at the time the radiation was emitted from the source. The surface area over which the emitted photons are spread was therefore also relatively small, but with the expansion the radiation was spread

over a larger area thus causing a dimming effect. The flux density is given by:

$$S = \frac{F}{4\pi D(z)^2(1+z)^2}, \tag{2.13}$$

normally the *luminosity distance* is defined as $D_L = D(z) \times (1+z)$. For a flat space-time ($\Omega = \Omega_M + \Omega_\lambda = 1$) the full expression for the luminosity distance is (Longair 1998; Dahlén 2002):

$$D_L = \frac{c(1+z)}{H_0} \times \int_0^z ((\Omega_M * (1+z')^3 + \Omega_\lambda)^{-1/2}) dz', \tag{2.14}$$

Ω_M is the contribution from matter (baryonic and dark) to the density parameter and Ω_λ is the "dark energy" contribution (a $\Omega_\lambda > 0$ means that the universe is expanding at an accelerated rate). For a thorough review of cosmological parameters and their definitions see Longair (1998).

When the fluxes are converted into magnitudes, the luminosity distance (denominator in equation 2.13) becomes the distance modulus (Dahlén 2002),

$$DM = 5\ log_{10}(D_L) - 5, \tag{2.15}$$

with D_L in parsecs. Therefore, for a given cosmology the distance modulus can be computed for the redshift under consideration.

2.4.2 K-correction

When redshifted galaxies are observed in a limited wavelength band (i.e. filter) the measured part of the spectrum is not the same as when observing a local (low redshift) galaxy (see figure 2.5). To compute the rest-frame magnitude in a certain filter this effect has to be taken into account. For the example in figure 2.5 the K term will be quite large (~ 1.4 magnitudes), but could also be almost nonexistent for certain parameter combinations.

When computing the K-correction for a galaxy, the SED of the galaxy type is needed (the photometric redshift code normally provides the type), as well as the filter transmission function and the redshift of the source. Normally the SED's used are empirical averages over a lot of local galaxies (e.g. Coleman, Weedman &Wu 1980; Kinney et al. 1996). The SED is redshifted to the redshift of the galaxy and convolved with the filter function. To get the corrections in AB magnitudes the filter functions for the different bands are first convolved with a flat spectrum. The resulting functions are then integrated to give model magnitudes which are normalized so that $V = 0.02$ (Dahlén 2003, priv. comm.). The K-correction of the galaxy ($K(z, F, SpT)$ in equation 2.11) is then given by subtracting the model magnitude at $z = 0$ from the model magnitude at the redshift of the galaxy.

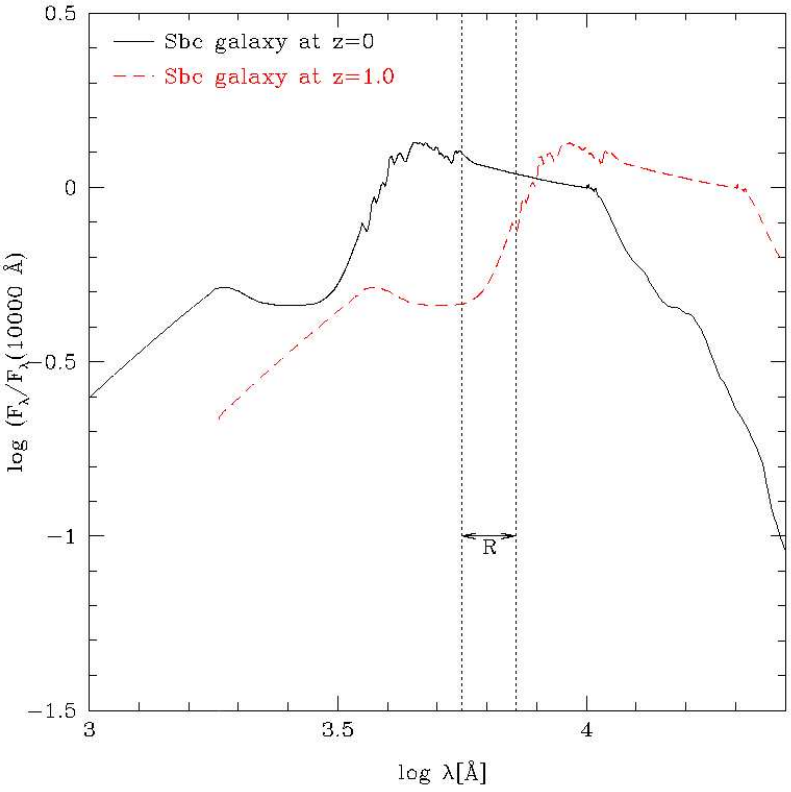

Figure 2.5: This figure demonstrates the concept of K-correction. The observed flux in the R band is different for the same galaxy at $z = 0$ and at $z = 1$. The Sbc galaxy SED is from Coleman, Weedman &Wu (1980) and the dotted lines mark the FWHM range of the WFI R band (Arnouts et al. 2001).

2.5 Theory of galaxy formation and evolution

2.5.1 Galaxy types and star formation

Galaxies are normally classified on the basis of their morphology. The so called Hubble diagram divides galaxies into late and early types, with spiral galaxies (designated Sa, Sb, Sc and Sd where abcd states how tightly the spiral arms are wound) and irregular galaxies (Im) as late types and elliptical (E0, E1,..., the numbers mark how elliptical, 0 being circular, the galaxy is) and lenticular galaxies (S0) as the early types. For more material on the Hubble diagram and galaxy morphologies consult any basic astronomy text. In reality, there is more to the galaxy types than just the differing morphologies. The amount of dust in the galaxies is different which directly influences the amount of internal extinction in the galaxies. But even more important, the presence of dust makes it possible for

cool molecular clouds to form; these clouds are the birthplaces of new stars. This also means that the different galaxy types have different SED's (cf. chapter 2.3).

Elliptical galaxies are the most dust-free galaxies and exhibit very little star formation activity. When galaxies age they grow redder and redder because the blue stars live a shorter (but brighter) life. Elliptical galaxies resemble the bulges of spiral galaxies, they both contain old red stars. Spiral galaxies contain quite a lot of dust and gas in the arm regions, this makes the spiral arms a good environment for stellar birth. The colours of spirals are thus much bluer than the ellipticals. The other late galaxy type are the irregular galaxies, which are often companions to larger galaxies, their irregular morphology is sometimes the result of a merger in process, but not always. Their dust content vary, some irregulars have been stripped of gas, most of them are quite blue which indicates that star formation is taking place. Since they are also quite dust-rich one has to consider reddening and extinction by the dust when studying these type of objects. Among the irregular and spiral galaxies there exist another class of intriguing objects, namely *starbursts*. These galaxies are characterized by their huge star formation rates (SFR), which can be an order of magnitude higher than the spiral galaxy SFR.

The stellar content of a galaxy can be modeled by using a given initial distribution of stars of different masses (an *Initial Mass Function*, IMF) and letting the stars evolve. The shape of the IMF, $\Upsilon(\mathcal{M})$ is given by a power law:

$$\Upsilon(\mathcal{M})d\mathcal{M} = c\mathcal{M}^{-\xi}, \tag{2.16}$$

where c is a normalization constant, M mass and $\xi = 2.35$ for the Salpeter IMF (Salpeter 1955). The distribution is finally determined by assuming a lower and upper mass cut-off. In general, the lower cut-off is set to $0.1\mathcal{M}_{\odot}$ and the upper to $125\mathcal{M}_{\odot}$ (Bruzual & Charlot 1993), which is what I have adopted in this work.

2.5.2 Galaxy formation and evolution

The universe is isotropic and homogeneous, the existence of stars and galaxies seem to contradict this, but it is all a question on which scales this statement is valid. The origin of all structure in the universe are small fluctuations in the energy distribution that exist after the recombination phase ($\sim$ 1 million years after the Big Bang). In the pre-recombination universe small instabilities form in the otherwise isotropic radiation, perhaps as quantum fluctuations, perhaps they were remains of processes in an earlier era. The spectrum of fluctuations, if there are more fluctuations on the large scale than on the small, will have a large influence on the formation of structure. However, both theory and observations, point to that fluctuations have the same probability at all scales, i.e. the universe is *self-similar*. Which instabilities that collapse and start to form bound systems is instead determined by the radiation transport in the systems. An instability will not collapse if there is radiation which can escape it. Different theories give

totally different formation scenarios for galaxies and galaxy clusters (see Peebles 1993; Longair 1998).

In the *top-down* scenario the collapse start on very large scales, cluster sized structures are the first to collapse. From the larger structure galaxies collapse and start to form stars. This scenario is explained by using so called *hot dark matter* (HDM), mainly in the form of neutrinos left over from the Big Bang. Instabilities are rapidly damped out by the weakly interacting neutrinos which transport energy away from all but the very largest fluctuations. Galaxies and smaller structure then form from fragmentation and instabilities in the large scale structure. This model was proposed by Zeldovich and colleagues in 1980 (see Zeldovich 1993). The main problems of this theory is that it predicts too much large structure compared to observations and that the formation of galaxies is predicted to be a pretty late event in the history of the universe.

The other important formation theory is the *bottom-up* scenario where small galaxies are the first to collapse and then larger structure is built up through *hierarchical clustering* (Press & Schechter 1974; Cole et al. 2000). The bottom-up scheme requires the dark matter to be cold (CDM model), this helps fluctuations of all sizes to survive into the post-recombination era (Peebles 1983, 1993). The smallest fluctuations are then the first to collapse and larger structure is built up by the smaller "building blocks". Galaxy merging is thus very important in this scenario. Currently the most favored theory is a variation of the CDM model, the λCDM model, i.e. cold dark matter with a "dark energy" component. Using N-body simulations Cole et al. (2000) (among others) have shown that this model fit the spectrum of structure well though it still remains to be seen whether the resulting merger rate and luminosity evolution is consistent with observations of high and medium redshift galaxies.

2.5.3 Observing galaxy evolution

Observations of galaxy populations at all redshifts can provide us with well needed observational data. Models of galaxy evolution and merging can be compared with the observationally found counts of galaxies (Metcalfe et al. 2001; Bershady, Lowenthal & Koo 2001). The rest-frame colour distribution of galaxies can be analyzed and compared to models (Wolf et al. 2003; Bell et al. 2003). Another statistical measure of the galaxy population is the *Luminosity Function* (Binggeli, Sandage & Tammann 1988; Longair 1998), LF hereafter. The LF, $\Phi(M) = n(M)dM$ (M absolute magnitude) is defined as the space density of galaxies with intrinsic luminosities in the range $M + dM$. I will use the Schechter parameterization of the LF which is given by:

$$\Phi(M) = 0.92\Phi^* \exp\left(-0.92(\alpha+1)(M-M^*) - \exp[-0.92(M-M^*)]\right) dM, \quad (2.17)$$

Φ^* is a normalization factor which fixes the space density of galaxies, M^* characterizes the break at high luminosities of the LF and α determines the slope of the

power law. Both M^* and Φ^* depend on the chosen cosmology.

The luminosity function is used when producing models of galaxy populations. The parameters of equation 2.17 can be found by fitting the function to large surveys of local galaxies. The locally obtained parameters are then used to model galaxy populations at higher redshift. The LF itself is of course also very interesting. Large surveys of galaxies at different redshifts can be used to obtain luminosity functions for different galaxy types and redshifts, and luminosity evolution of the galaxies can be studied (e.g. Dahlén 2002; Wolf et al. 2003; Chen et al. 2003). The luminosity function for different galactic "environment" (i.e. clusters, field etc.) are different (Binggeli, Sandage & Tammann 1988). Comparisons of the LF's can help us understand the similarities and differences of galaxy evolution in a dense versus a sparse environment.

3

The Data

The data was taken from the publicly available ESO Imaging Survey (EIS) deep public survey of Chandra Deep Field-South (CDFS) centered at RA $\sim 3^{h}32^{m}$, Dec $\sim$ -27 °48′. This field is selected as an "empty" field with few luminous galaxies, the total area covered when the survey is completed will be $\sim$2 sq. degrees. The currently available data covers $\sim$0.25 sq. degrees in the optical filters and $\sim$0.15 in infrared filters. The observations were made with the Wide Field Imager (WFI) at the Max-Planck-ESO 2.2-m telescope (UBVRI), and with the SOFI instrument at the New Technology Telescope (NTT) (JK_s) both at La Silla in Chile. The WFI has eight $2k \times 4k$ CCDs with a total field of view of $34' \times 33'$, and a pixel scale of 0.238 ″/pxl. SOFI has a pixel scale of 0.292 ″/pxl and a field of view of $4.9' \times 4.9'$. The total infrared images are composed by 16 tiles. Observations were made in seven broad band filters (corresponding to Johnson-Cousin filters UBVRIJK_s, see figure 2.1). A more detailed description of the observations and data reduction, as well as source catalogues can be found in Arnouts et al. (2001) (for the optical data) and Vandame et al. (2001) (for the infrared data). Very bright sources (only stars in this data) have been masked in the images (see figure 3.1).

3.1 Source detection and photometry

Since I wanted to find photometric redshifts for the galaxies in the field, I performed my own source detection and photometry on the data in order to get accurate colours. Source detection was done with SExtractor (SE) (Bertin & Arnouts 1996). Detection was performed separately in each band on the images using the provided weight maps after convolving with a Gaussian with FWHM roughly equal to the seeing in each band. The detection parameters in SE is the detection threshold (a flux limit for a pixel to be considered detected) and the minimum area in pixels (the number of detected pixels a "real" object has to contain). These parameters

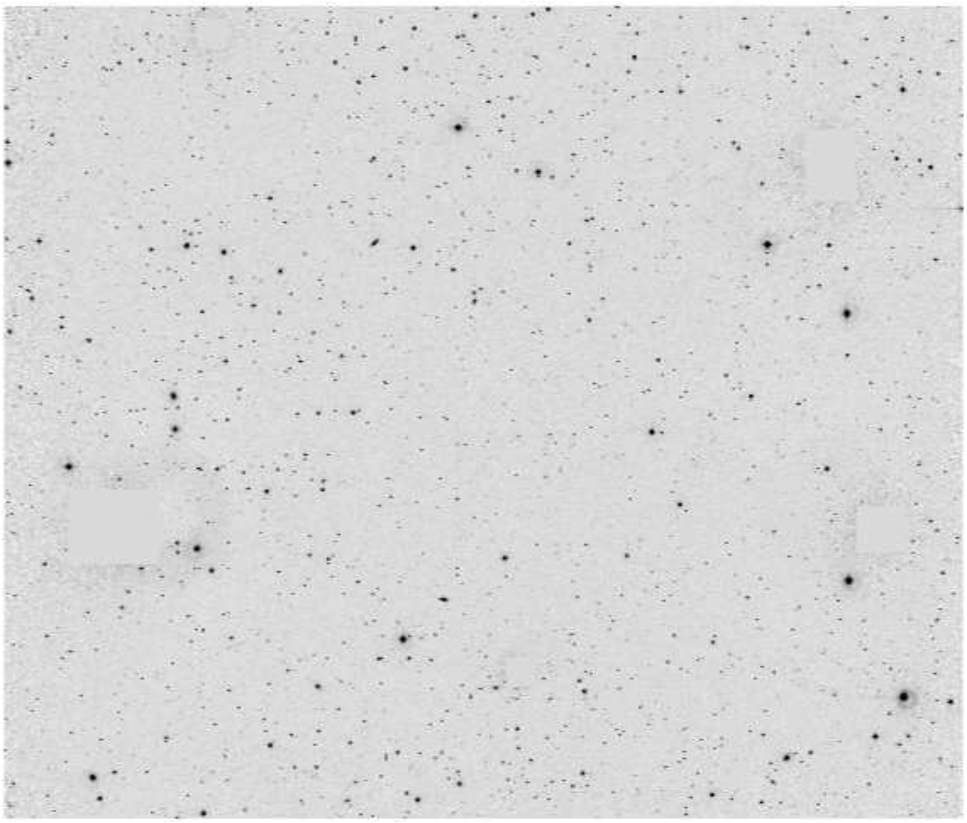

Figure 3.1: I band image of Chandra Deep Field South from the EIS Deep Public Survey. Masked regions contain saturated stars.

need to be finely tuned to detect faint galaxies, but at the same time minimize the number of spurious detections.

To optimize the parameters with respect to the number of spurious detection SE was used on both the image under consideration and on a mock image (the inverted image). Since the noise is mainly Gaussian the number of spurious detections is expected to be the same in both images, since there are no real negative sources. Using this technique I found that the optimal detection threshold was between 0.55(B)-0.8(R) times the noise level (rms) and the minimum area between 8(I)-12(B) pixels. For the infrared data the detection threshold was 0.8 times the noise level and the minimum area was 7 pixels. With these parameters the number of spurious detections was $\lesssim$ 5% in all bands. A comparison with the number of detections in the optical bands by Arnouts et al. (2001) show that my choice of parameters are slightly more conservative.

SExtractor also does photometry on the detected sources. Total magnitudes of the sources are estimated with SE's MAG_AUTO measurement, which is a Kron aperture (Kron 1980). This underestimates the total flux of the sources by about

6 % (Bertin & Arnouts 1996), but is widely used as a total magnitude in other large surveys (e.g. Wolf et al. 2003), thus no correction for this was made. To obtain good photometric redshifts the same part of the object's radial brightness profile in all bands need to be measured. This means that the different seeing conditions in the bands becomes a problem. In order to solve this I convolved all the images to the same seeing (1.02″ in B band), and measured 3″ aperture magnitudes in all bands. I then used SE's "dual" mode, i.e. detecting in the original images but doing photometry in the convolved image.

The resulting photometric catalogues were then matched in RA and Dec. The final catalogue includes 45 061 objects which are R-band selected, i.e. the objects found in the other bands were matched against the R-band and only objects which were detected in R and had errors smaller than 1σ were kept. Stars were removed from the sample by using SExtractor's CLASS_STAR value. This value is determined mainly from comparing the point spread function to the seeing in the image and uses an artificial neural network. Objects with CLASS_STAR > 0.95 in any of the three bands VRI (chosen for the good seeing conditions in these bands) or a mean CLASS_STAR in the three bands larger than 0.5 were considered to be stars (c.f. Arnouts et al. 2001).

The magnitude zeropoints used are the extinction corrected zeropoints provided by the EIS image headers for each image. The magnitudes were also color-corrected using the correction terms found by Arnouts et al. (2001), then transformed to AB magnitude system using the following relations; $U_{AB} = U + 0.80$, $B_{AB} = B - 0.11$, $V_{AB} = V$, $R_{AB} = R + 0.19$, $I_{AB} = I + 0.50$, $J_{AB} = J + 0.90$, $K_{AB} = K_s + 1.84$. The magnitudes have not been corrected for galactic absorption. Arnouts et al. (2001) uses corrections ranging between 0.05 mag (U) to 0.02 mag (I). The number of detected objects, seeing and limiting magnitudes in each filter is given in table 3.1. The seeing-corrected aperture magnitudes have been used to produce the photometric redshifts. Rest-frame magnitudes and those used in number counts are based on the total magnitudes (SE's MAG_AUTO) measured on the original frames.

3.2 Completeness

The completeness of the data can be investigated in a number of different ways. One possible way is to implant artificial galaxies into the images with known magnitudes. Then the same detection procedure is performed on the images with artificial galaxies as on the original image. The completeness at a certain magnitude is then the percentage of the mock galaxies that are detected by the detection algorithm. This is the procedure used by e.g. Metcalfe et al. (2001) and Minezaki et al. (1998). The problem with this method is that you have to assume a brightness profile and morphology of the artificial galaxies and these approximations will not always cover the entire range of galaxy types. The completeness could in principle

Table 3.1: Limiting magnitudes in the 7 filters, calculated using equation 2.6 in a 2× FWHM aperture (AB magnitudes). Seeing for UBVRI bands are from Arnouts et al. (2001), for J and K_s the reported values is a mean for the 16 patches (Vandame et al. 2001). The number of objects (N_{obj}) are objects brighter than the 5σ magnitude limit in each band.

Filter	m_{lim} (5σ) (mag)	Seeing (FWHM) arcsec	N_{obj}
U	25.9	0.98	14 516
B	26.7	1.02	32 611
V	25.9	0.97	26 594
R	25.9	0.86	34 316
I	25.1	0.93	21 730
J	23.6	0.82	5 099†
K_s	22.8	0.77	2 924†

†The area covered in the infrared bands is smaller than in the optical bands, see text.

be different for different kinds of galaxies. To make an accurate determination of the completeness one would need to model a mixed galaxy population with ratios of different morphologies and brightness profiles close to the observed ratios in the data set.

Another method is to use the so called "postage stamp" method where cut-out images of galaxies are inserted into the original image (e.g. Arnouts et al. 1999; Yan et al. 1998; Bershady, Lowenthal & Koo 2001). A number of fairly bright galaxies are cut out from the image and artificially dimmed to the magnitude studied. They are then implanted into the image again and detection is done on the mock image. The completeness is then the percentage of the artificially dimmed galaxies detected. When using this method one be aware that it is easy to bias the data by only selecting galaxies of a certain type as postage stamps. It might also be a problem to use bright galaxies as templates, since the bright (and often close) galaxies might be inherently different than the faint galaxies close to the completeness limit (Saracco et al. 1999).

Instead, I choose to use the method of Saracco et al. (1999). The raw number counts of galaxies in magnitude bins (bin size of 0.5 mag) is computed. The original image is then dimmed by dividing the fluxes in the image by a factor corresponding to the magnitude shift under consideration. The noise level in the image is kept at the same level as in the original image (using IRAF task `mknoise`). Then source detection is done on the dimmed image and the raw number counts are computed in the same magnitude bins as before. The results of this analysis can be found in table 3.2. The C ratio (inverse of the completeness percentage) for a

Table 3.2: Differential number counts in the B and I bands derived from the sample with sources having $S/N \geqslant 5$. The errors σ_N includes the Poissonian error on the raw counts (n) and the uncertainty in the completeness correction factor C. Magnitudes are in AB system.

B	n	C	$N/0.5mag/deg^2$	σ_N
17.5	6	1.00	19	8
18.0	8	1.00	25	9
18.5	20	1.00	63	15
19.0	20	1.00	63	15
19.5	54	1.00	169	24
20.0	86	1.00	270	31
20.5	121	1.00	379	36
21.0	160	1.00	502	42
21.5	238	1.00	746	51
22.0	415	1.00	1301	67
22.5	762	1.00	2389	91
23.0	1264	1.00	3962	117
23.5	2351	1.00	7370	160
24.0	3759	1.00	11784	202
24.5	5362	1.05	17649	252
25.0	6647	1.14	23754	303
25.5	6545	1.82	37341	469
26.0	3136	7.69	75598	1351
26.5	1629	22.93	117094	2901
27.0	28	939.75	164972	31177
I	n	C	$N/0.5mag/deg^2$	σ_N
15.5	2	1.00	6	5
16.0	4	1.00	13	7
16.5	10	1.00	31	10
17.0	18	1.00	56	14
17.5	29	1.00	91	18
18.0	59	1.00	185	25
18.5	89	1.00	279	31
19.0	140	1.00	439	39
19.5	221	1.00	693	49
20.0	405	1.00	1270	66
20.5	676	1.00	2119	86
21.0	1049	1.00	3288	107
21.5	1369	1.00	4292	122
22.0	1819	1.00	5702	140
22.5	2387	1.05	7857	168
23.0	3338	1.08	11301	204
23.5	4111	1.27	16367	263
24.0	3632	2.73	31082	519
24.5	1781	14.76	82406	1953
25.0	582	56.64	103337	4284

magnitude bin (centered at M_c) is then the number of galaxies in the bin that has been shifted (centered at $M_c - \Delta M$, from the original image) over the number of galaxies detected in the M_c bin in the dimmed image.

The uncertainty in numbers is formed by quadratically summing the contributions from the Poissonian errors ($\sigma_n = \sqrt{n}$) and the completeness factor ($\sigma_C = (N/n)\sigma_n$). There is also a contribution to the uncertainty from clustering fluctuations, which according to Saracco et al. (1999) might be as large as the Poisson error for bright magnitudes and even higher for fainter magnitudes (this is for J and K_s magnitudes and a field of view radius of $\sim 150''$). The clustering fluctuation errors are, however, dependent on the size of the field, for larger fields the contribution is expected to decrease in relative to the total number of sources. The errors in table 3.2 does not include these errors.

3.3 Photometric redshifts

I applied the BPZ code on 21 053 galaxies, all with total magnitudes brighter than the 3σ limit in I ($I \leqslant 25.17$). The redshift distribution can be found in table 3.3 and a histogram of the redshift distribution is found in figure 3.3. The prior used is the same used by Benítez (2000), the prior is calibrated against the HDF-N data using 737 galaxies with $20 < I < 27$ (Williams et al. 1996) and 591 galaxies from CFRS data (Lilly et al. 1995a; Crampton et al. 1995) with $20 < I < 22.5$. I also computed the redshifts using HyperZ (Bolzonella, Mirales & Pelló 2000) with the same templates as those used in BPZ (see chapter 2.3.3). A comparison of the models with spectroscopic redshifts (provided by the GOODs team) is shown in

Table 3.3: Distribution of the sample galaxies in redshift bins of 0.2 (galaxies at the limit go into the lower bin). Errors, σ_{nz}, are Poisson errors.

z	n_z	σ_{nz}
$\leqslant 0.2$	3943	63
0.3	3572	60
0.5	4203	65
0.7	3057	55
0.9	1470	38
1.1	1270	36
1.3	1120	33
1.5	1019	32
1.7	246	16
1.9	75	9
> 2.0	1078	33

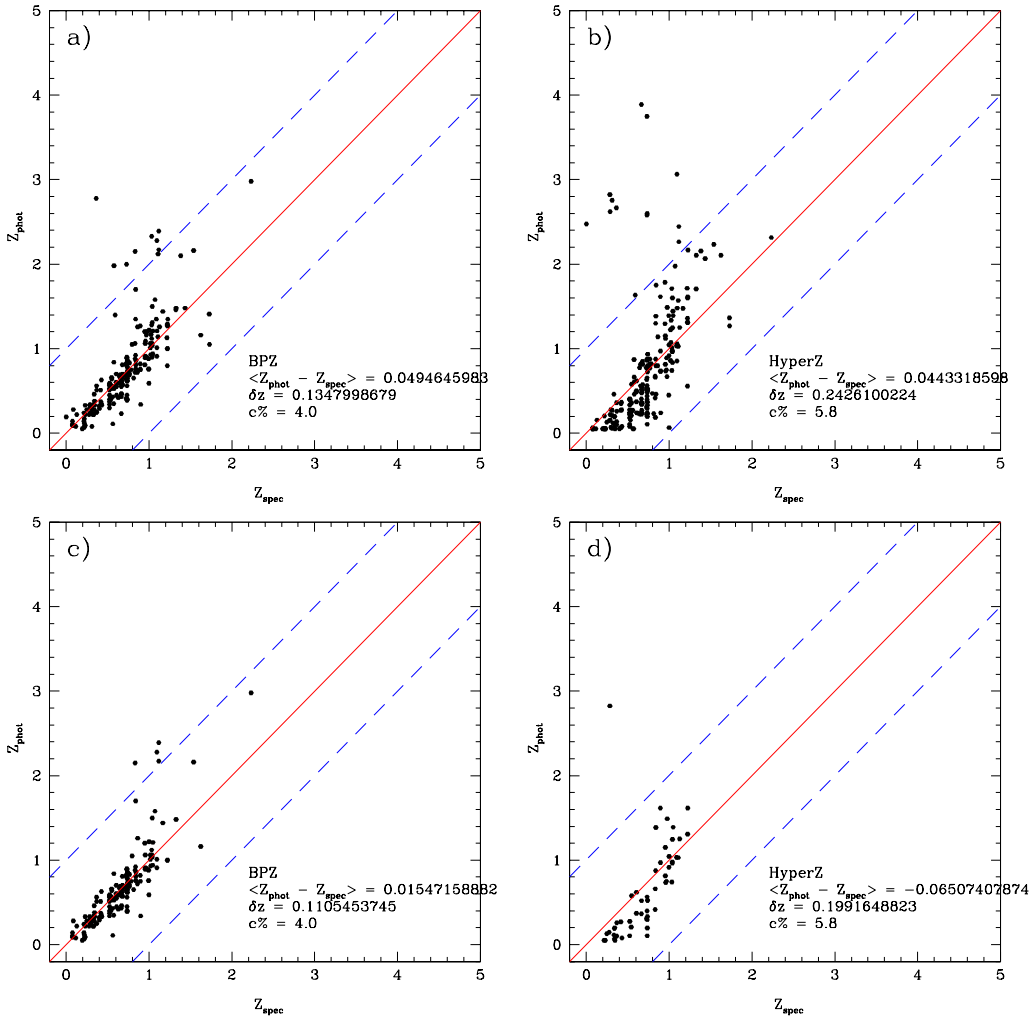

Figure 3.2: Comparison of the photometric redshifts with spectroscopic redshifts for 226 sources. a) BPZ for all 226 galaxies with redshift, b) HyperZ for all 226 galaxies, c) BPZ for 176 galaxies with $P(\chi^2) > 0.68$, d) HyperZ for 54 galaxies with $P(\chi^2) > 0.68$. It is clear that BPZ estimates the redshifts better than HyperZ, both in terms of catastrophic redshifts (c%, computed for the entire set for all panels) and redshift accuracy (δz).

figure 3.2. The comparison with spectroscopic redshifts is for 226 galaxies up to $z \sim 2.3$ and shows that the photometric redshifts have relatively small errors. For BPZ the mean of the redshift residuals, $< \Delta z_{phot} >= 0.05$ ($\Delta z_{phot} = z_{phot} - z_{spec}$) and the rms of the quantity $\Delta z_{phot}/(1 + z_{phot}) = \delta z$ is 0.13. This is comparable

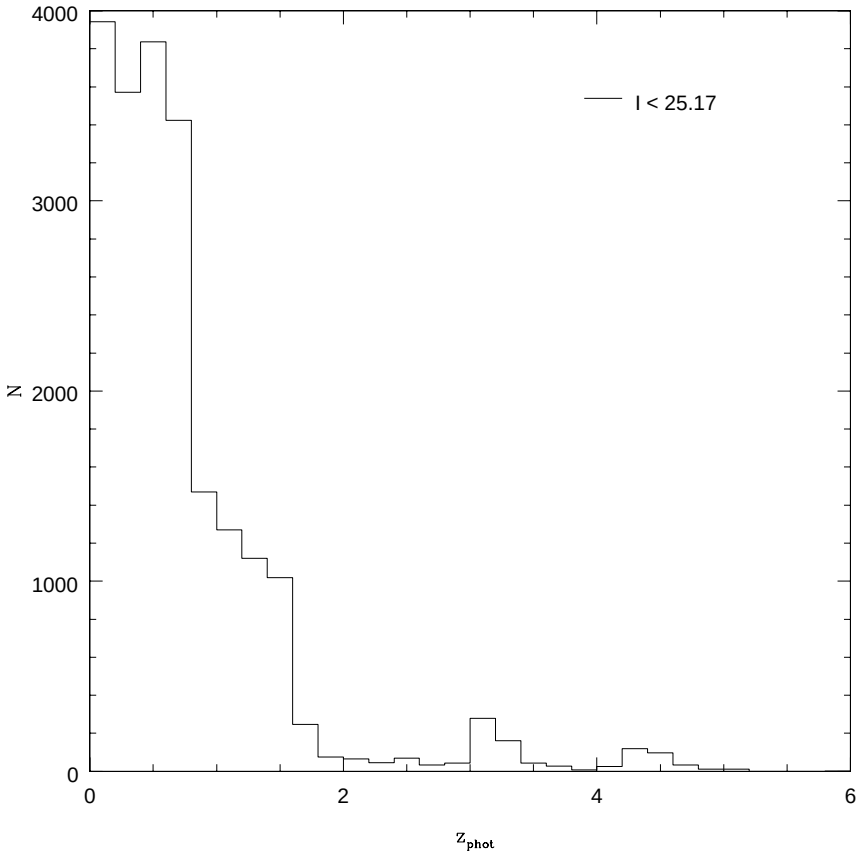

Figure 3.3: Redshift distribution for galaxies brighter than the 3σ magnitude limit in I. The small peaks at $z \sim 3$ and $z \sim 4.5$ are most probably spurious due to template mismatching.

to the work of other authors (Benítez 2000; Wolf et al. 2003; Chen et al. 2003). The HyperZ result is not as good as the BPZ result, it suffers more from template mismatching and also seem to yield systematically low redshifts for $0 < z \lesssim 0.5$. I therefore choose to use the BPZ results as my best-fit photometric redshifts.

The cumulative redshift distribution is plotted in figure 3.4. Wolf et al. (2003) has investigated the redshift distribution completeness of their data and find that for faint limits in R ($R < 24$ in their case) a significant number of galaxies are lost. This is probably the case for our data as well and has to be taken into account when analyzing the redshift distribution of the sources. The median redshift for the sample is 0.57. The photometric zeropoints of the data (included in the FITS headers) have larger errors than what is reported in the headers (Mobasher 2003, priv. comm.) so the minimum errors in photometry used for determining the photometric redshifts were set to high values (from 0.25 for I band to 0.1 for B

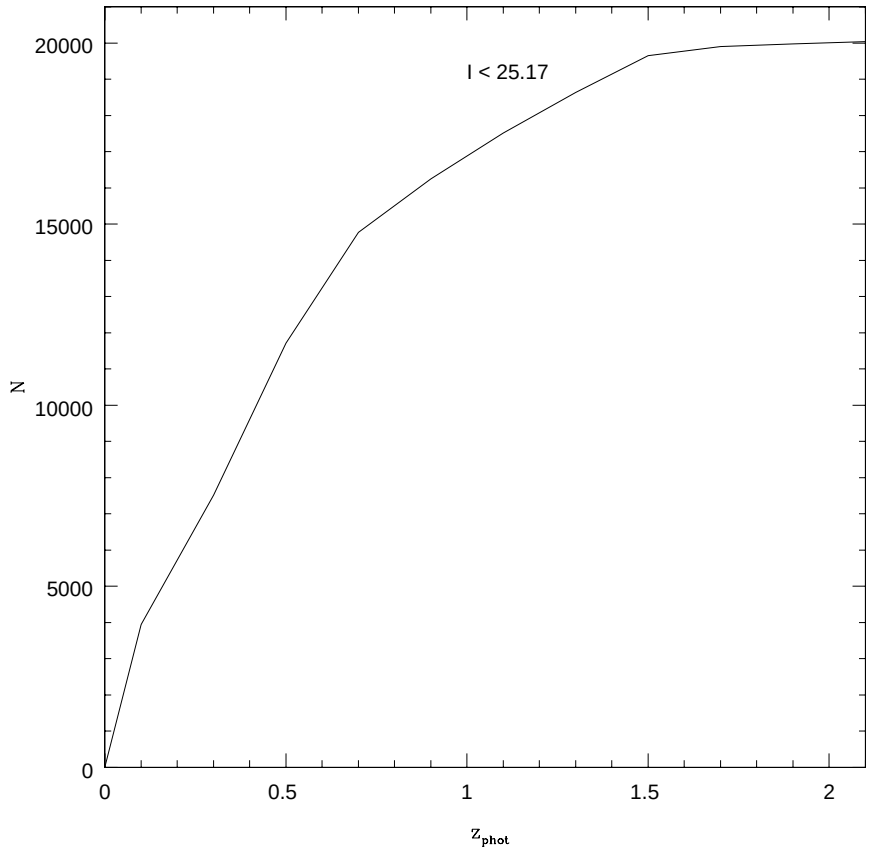

Figure 3.4: Cumulative redshift distribution of galaxies brighter than the 3σ magnitude limit in I.

band). The errors in the photometry directly influences the redshift confidence limits and the 68% confidence intervals for the sample galaxies become pretty large (mean range of ~ 1).

At redshifts less than 0.2 a large part of the sample have very large redshift confidence intervals (for $\gtrsim 50\%$ of the sample the 68 % confidence interval stretches up to $z \sim 3$). This is probably because of template degeneracy for galaxies with very faint magnitudes, since the problem becomes much worse if galaxies with fainter magnitudes than the current limit is considered. The small peaks in the redshift distribution at $z \sim 3$ and $z \sim 4$ (see figure 3.3) are very faint galaxies which lack good photometry in some of the bands, but most importantly in the U band. These galaxies might in fact be faint dwarf galaxies (ellipticals) at low redshifts which are erroneously classified as starbursts at high redshift. Figure 3.5 shows that the U band is in fact the discriminating band between elliptical galaxies at low redshift and starburst galaxies at $z \sim 3$. There is of course a population of

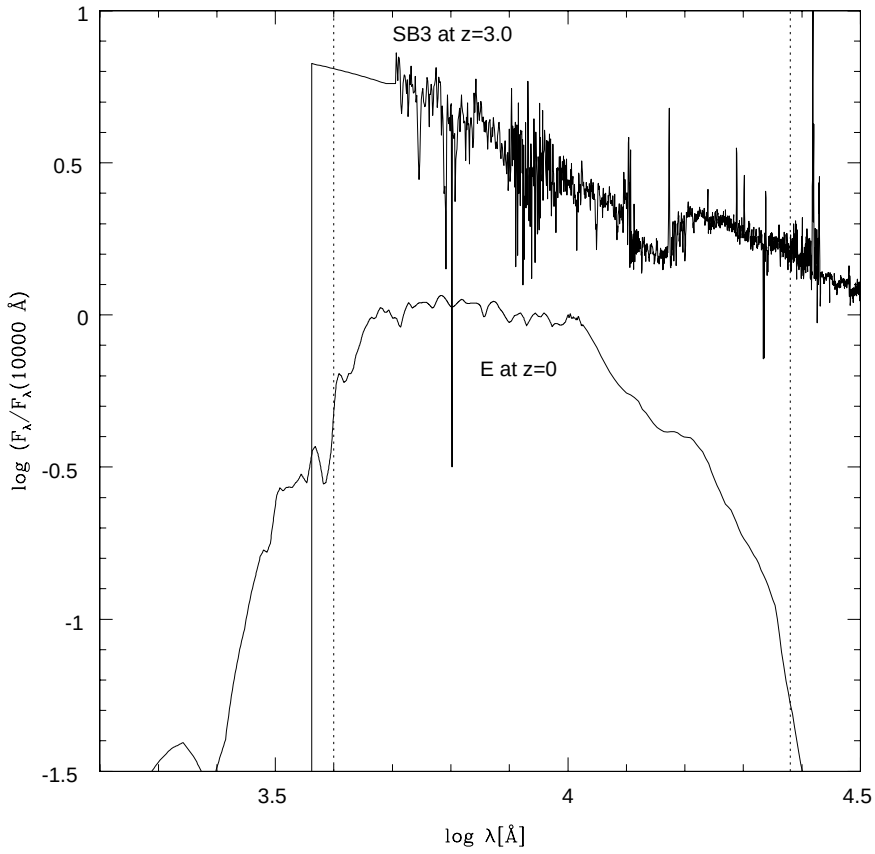

Figure 3.5: Comparison of template SED's from a low redshift elliptical galaxy (Coleman, Weedman &Wu 1980) and a starburst galaxy at $z = 3.0$ (SB3 from Kinney et al. 1996). The templates were both normalized at 10000 Å(restframe). The dotted vertical lines indicate the wavelength coverage of UBVRIJK$_s$ bands. The U band is closest to the left dotted line.

high-z galaxies (z$\gtrsim$ 3.5) that are next to impossible to detect in U (the so called U-dropouts), but it is very unlikely that all of the galaxies in the peaks are true U-dropouts. The photometric redshifts thus become very insecure for faint galaxies at $z \gtrsim 2.5$.

The chosen redshift range over which the restframe colour evolution is studied is therefore chosen to be $0.2 < z < 2.0$. Over this range the rms dispersion for the galaxies with spectroscopic redshifts is $\delta_z = 0.13(1 + z)$, and the number of catastrophic redshifts are low (c.f. Chen et al. 2003).

3.4 Rest-frame magnitudes

The absolute magnitudes of the 21 053 galaxies in my sample have been computed using the results from chapter 2.4. The distance modulus was computed using the given ($\Omega_M = 0.3$; $\Omega_\lambda = 0.7$; $h = 0.7$) cosmology for all redshifts between 0.01 and 6.0 (with a stepsize of 0.01). K-corrections were obtained for the WFI and SOFI filters, by convolving them with the SED's used in the photometric redshift estimation (Dahlén 2003 priv. comm.). Each galaxy was then classified to a specific SED using the best-fit from BPZ and the absolute magnitude was calculated using equation 2.11. The photometric redshift errors cause quite large errors in the absolute magnitudes (through the distance modulus and the K correction), but errors for the rest-frame colours are smaller since they are not affected by the errors in the distance modulus. The colour errors vary from galaxy type to galaxy type and are generally larger for lower redshifts but these variations are low. The errors in photometric redshift, $\delta z \sim 0.13$, translate into errors in the rest-frame colours, $\delta(U - V) \sim 0.3$.

Figure 3.6 shows the redshifts of the entire galaxy sample ($z < 2.0$) plotted against their I band absolute magnitude. The limiting magnitude used ($I_{AB} < 25.17$) is visible as the somewhat "fuzzy" limit to the right of the plot (from $M_I \sim -16$ at redshift 0.3 to $M_I \sim -21$ at redshift 2.0). This is consistent with the results for CDF-S of Wolf et al. (2003).

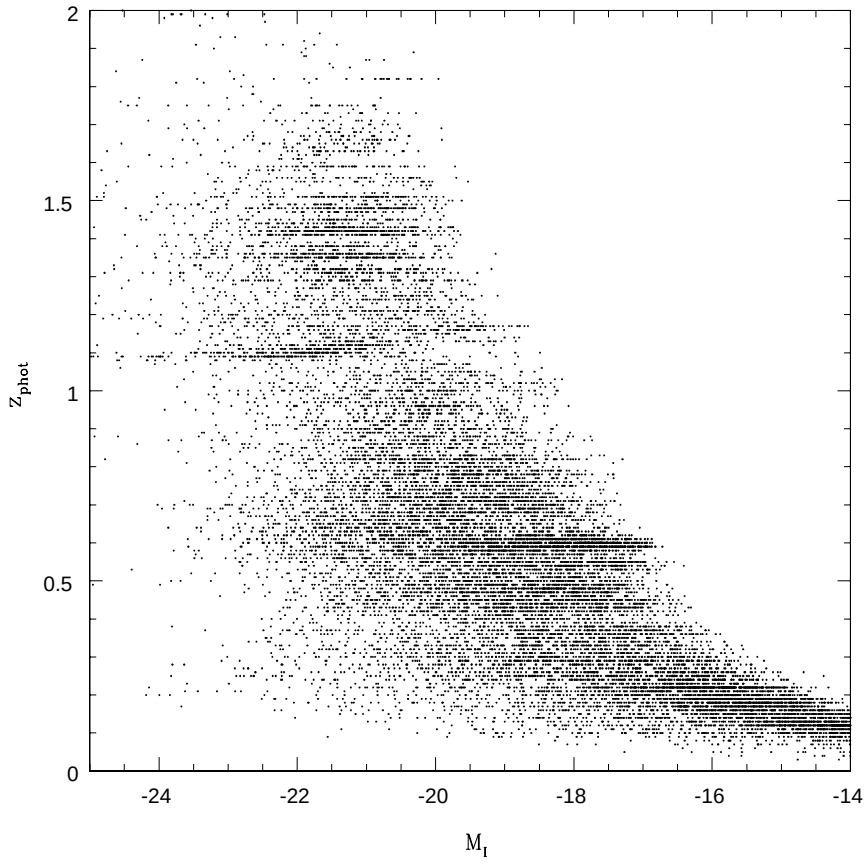

Figure 3.6: The redshifts vs the absolute magnitudes of galaxies brighter than the 3σ level in I band ($I_{AB} < 25.17$). The fuzzy limit at the right hand side of the figure correspond to the magnitude cut used (see text). Note the absence of strong "horizontal lines" in the plot, this means that the field does not contain any large clusters (c.f. Wolf et al. 2003).

4

Galaxy number counts

Number counts of galaxies can be used to probe both the properties of space-time and how galaxies evolve. The problem has then of course been to separate the effects of cosmology and galaxy evolution on the observed counts. During the latest years other observations and methods have made it possible to determine the cosmological parameters with unprecedented accuracy (e.g. SN cosmology, WMAP). Nagashima et al. (2002) find, using a hierarchical merging model, that λCDM parameters give a better fit than regular CDM to the observed counts, the models used in this work also use this type of cosmology. Keeping the cosmological parameters to fixed values give us the possibility to study the effects of galaxy evolution on the number counts. The raw (i.e. not normalized to a certain area nor corrected for incompleteness) number counts for the CDF-S in the seven filters used in this work is given in figure 4.1.

4.1 Number count models

The galaxy number counts can be modeled using stellar synthesis models. The models I have compared with have been produced with the code by Bruzual & Charlot (1993) in collaboration with Peter Weilbacher at University of Durham. Using this code the luminosity evolution of a galaxy can be modeled by assuming an IMF (see chapter 2.5), the formation redshift, the metallicity and the evolution of the SFR (also chapter 2.5). Bruzual & Charlot (1993) provides stellar libraries of colours for stars in any stage of their evolution, this is used to model the galaxy colours and photometry. To find the model counts we assume different LF's (see chapter 2.5.3 and table 4.1) for the galaxy types and integrate over the entire sample of galaxies.

We have considered three different models, two with luminosity evolution and one without (Weilbacher, 2003 priv. comm.). The non-evolution model is created

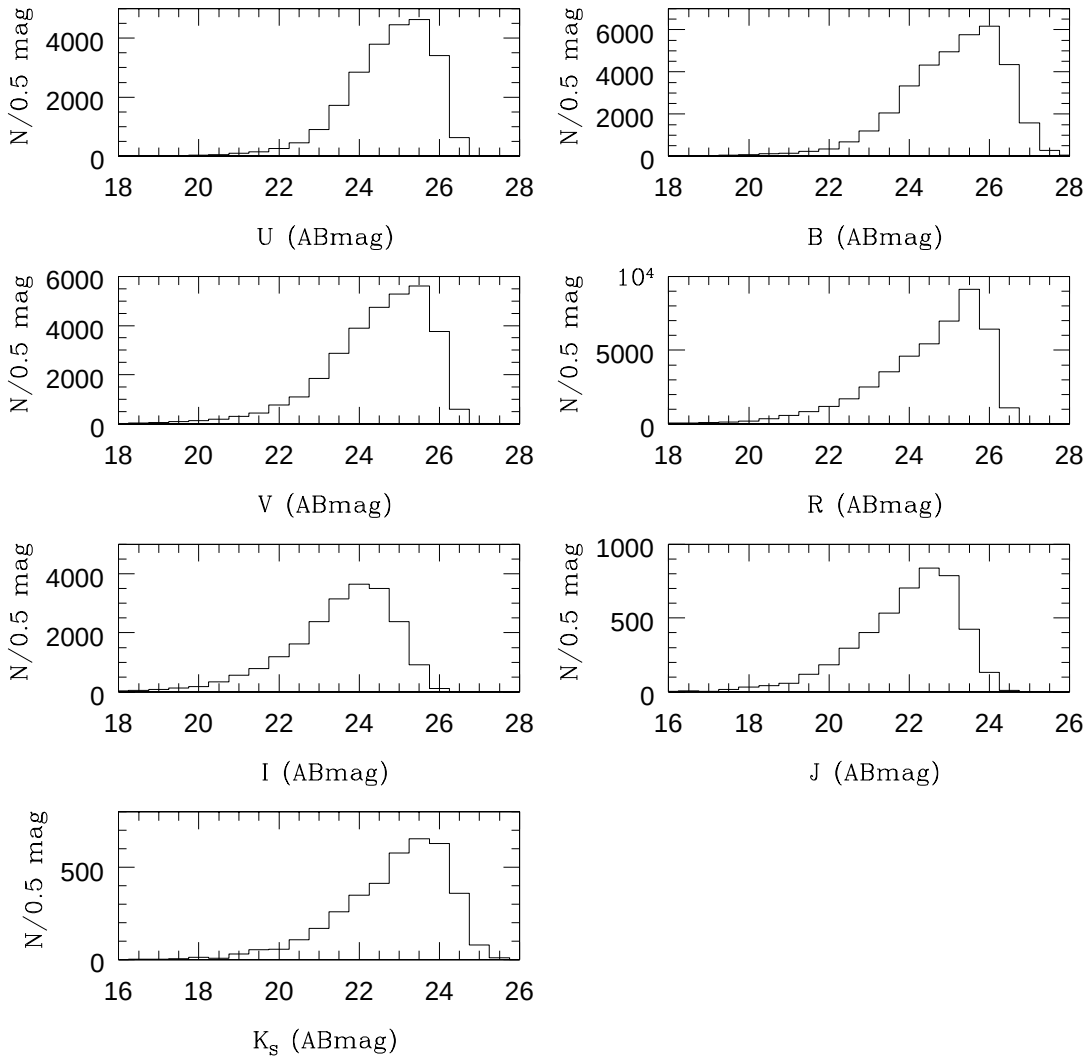

Figure 4.1: Galaxy number count histograms for the seven observed filters. Magnitudes are in AB system using a 5σ limit (see table 3.1). Note that for J and K_s the observed field is smaller.

at the formation redshift and have a constant SFR (high or low for the different galaxy types), but as the stars age, even a non-evolution model galaxy sample will undergo changes in luminosities. The models are of course also affected by the assumed cosmology (which directly determines the formation redshift as well). All models are computed using a Salpeter IMF (equation 2.16), solar metallicity, λCDM cosmology and a Schechter LF (equation 2.17) with parameters found in table 4.1. The two luminosity evolution models have the following properties:

1. Two different galaxy types are considered, E/S0 with a SFR decay time (τ_{SFR}) of 0.5 Gyrs and Sa/Sc/Sdm with $\tau_{SFR} = 9$ Gyrs.

2. Three galaxy types, E/S0 with $\tau_{SFR} = 0.5$ Gyrs, Sa/Sb with $\tau_{SFR} = 7$ Gyrs and Sc/Sdm with $\tau_{SFR} = 99$ Gyrs (in principle a constant SFR).

The output of the models are number counts in 0.5 magnitude bins for AB magnitudes normalized to 1 sq. degree.

4.2 Galaxy counts in B band

The obtained galaxy counts in B band (figure 4.2 and 4.3) agree very well with the work of other authors (Metcalfe et al. 2001; Huang et al. 2001; Yasuda et al. 2001). For the brightest magnitudes the count errors relative to the total number of objects are quite large, when the numbers increase the relative errors become much smaller. The faintest bins are heavily affected by incompleteness and the numbers become more uncertain there. These bins are probably affected by systematic errors in addition to the shown Poisson errors (see table 3.2), this has not been investigated.

A comparison of the counts with the models show that the counts at bright magnitudes are easily fit by any of the models. For fainter magnitudes (starting at around $B = 23$) the non-evolution models generally predicts too few galaxies, this is the famous "faint blue galaxy" problem (e.g. Ellis 2001). As can be seen in the figure the luminosity evolution models fit the counts better for the faint magnitudes, this is because the galaxies change their luminosities with time (the SFR of the galaxies change with age). Most of the numerous faint blue galaxies are very distant, this population will fade with time when using luminosity evolution of the type considered here. The two evolutionary models are very similar. Model 1 fits the data slightly better at faint magnitudes but slightly worse for the $B = 23 - 25$ range.

Table 4.1: Details of the luminosity functions used for modeling number counts. The parameters used are from Metcalfe et al. (2001). Magnitudes are in AB system. See equation 2.17 for details.

	E/S0	Sab	Sbc	Scd	Sdm
$\Phi^*_{noevol}(Mpc^{-3})$	0.00102	0.000509	0.000682	0.00030	0.00015
$\Phi^*_{evol}(Mpc^{-3})$	0.000927	0.000463	0.00062	0.000273	0.000136
α	-0.7	-0.7	-1.1	-1.5	-1.5
M^*_B	-20.85	-20.88	-21.22	-21.37	-21.38
$M^*_{I/Ks}$	-22.44	-22.26	-22.38	-22.21	-22.13

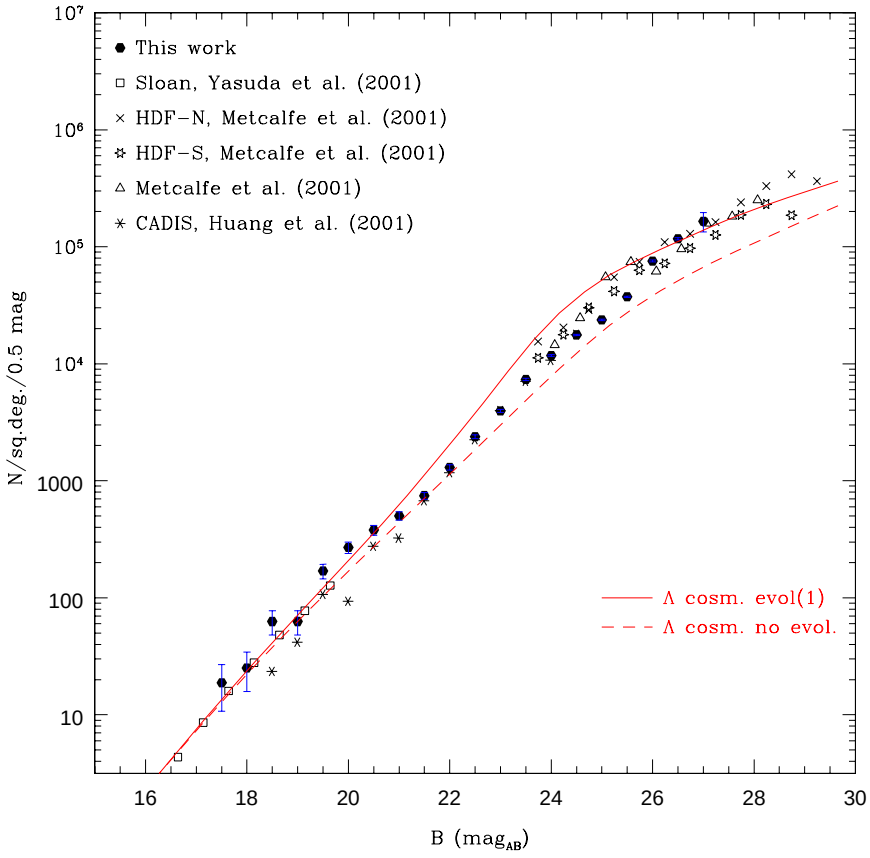

Figure 4.2: Differential number counts in B band with completeness corrections as in table 3.2. Comparison with data from Metcalfe et al. (2001); Huang et al. (2001); Yasuda et al. (2001). **Model number 1** (see chapter 4.1) is used in this plot. Magnitudes are in AB system using a 5σ limit (see table 3.1).

The problem with the two models is also clearly seen in figure 4.2 and 4.3, the counts at intermediate magnitudes are overpredicted. There are different approaches to solve this problem, one is to include the effects of dust in the galaxies in the models (Campos 1995). Metcalfe et al. (2001) uses a non-Salpeter IMF to model the counts and obtain a good fit to the observations, but this IMF is not supported by observations of local galaxies. Nakata et al. (1999) have modeled field galaxy evolutions using pure luminosity evolution and found that a single-burst model is inconsistent with observed counts of galaxies. Hierarchical models of galaxy formation and evolution (Cole et al. 2000), including the effects of dust, might be the solution. The faint distant galaxies disappears by merging together, so the counts at bright and intermediate magnitudes are kept at the observed levels while still having a large faint blue population.

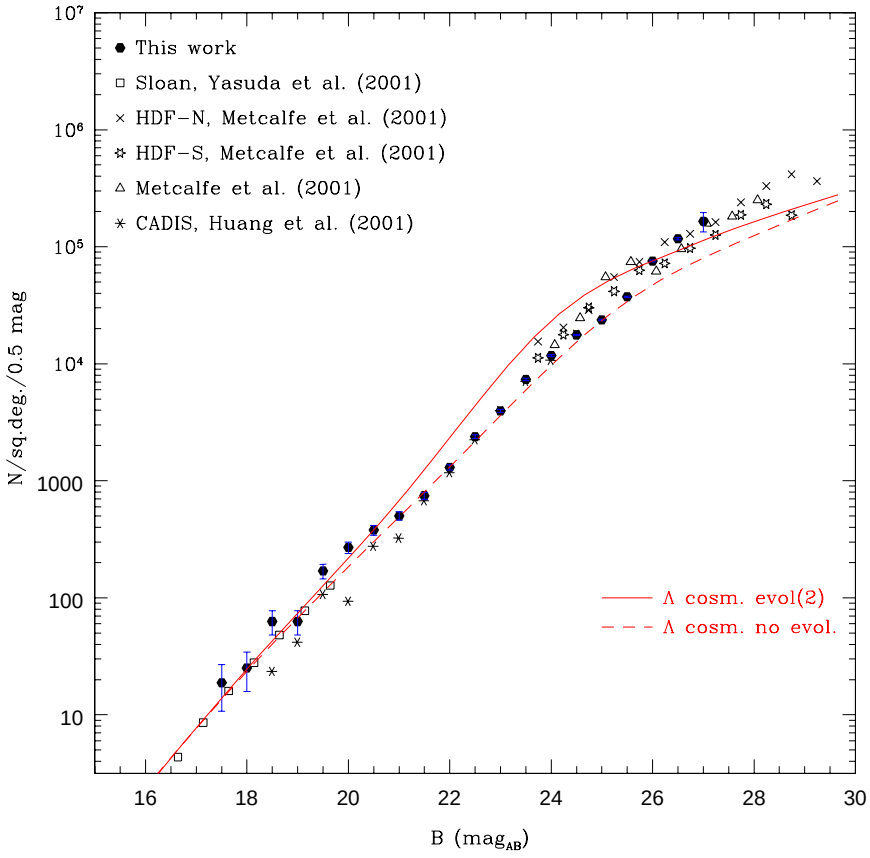

Figure 4.3: Differential number counts in B band with completeness corrections as in table 3.2. Comparison with data from Metcalfe et al. (2001); Huang et al. (2001); Yasuda et al. (2001). **Model number 2** (see chapter 4.1) is used in this plot. Magnitudes are in AB system using a 5σ limit (see table 3.1).

4.3 Galaxy counts in I band

The I band counts (figure 4.4 and 4.5) also agree very well with work done by other authors (Postman et al. 1998; Metcalfe et al. 2001; Yasuda et al. 2001), the discussion on errors in the previous section applies to this data as well. One major difference compared to the B band is that the departure from the non-evolution model sets in for fainter magnitudes (at around $I = 24$), this is because the blue bands are much more sensitive to changes in the SFR (Metcalfe et al. 2001).

The excess of faint galaxies for the non-evolution model is evident in the I band counts as well. The problematic "bump" at intermediate magnitudes ($I = 22 - 26$) becomes even more obvious, especially for model 1. That this bump is less accentuated in the B band might in fact provide us with a clue to why it

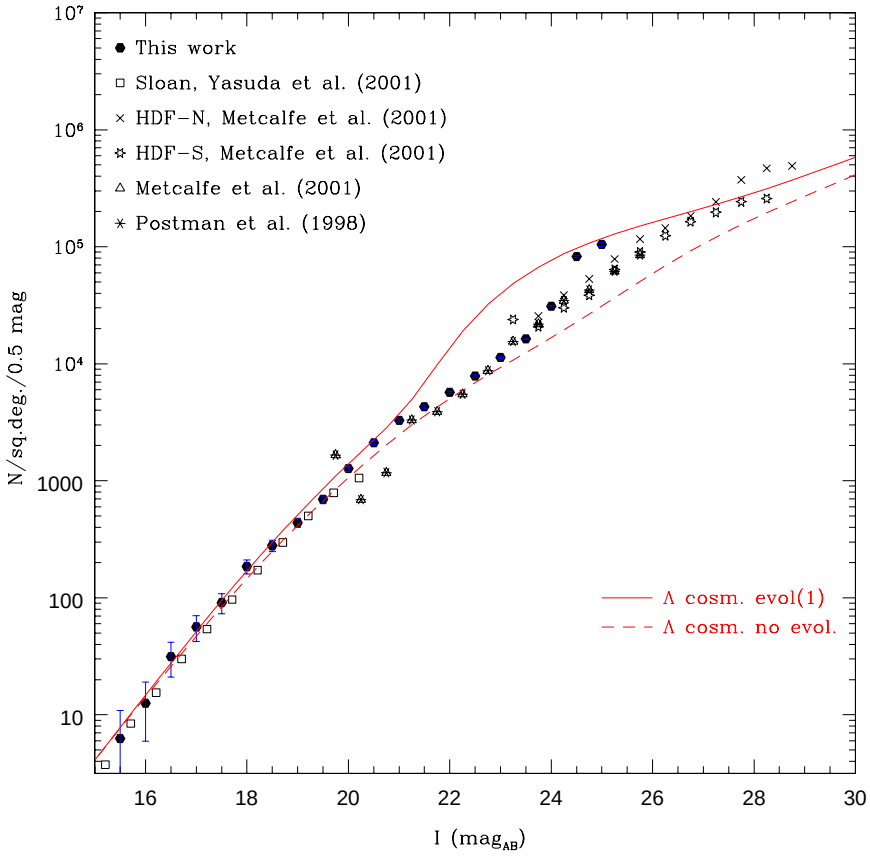

Figure 4.4: Differential number counts in I band with completeness corrections as in table 3.2. Comparison with data from Postman et al. (1998); Metcalfe et al. (2001); Yasuda et al. (2001). **Model number 1** (see chapter 4.1) is used in this plot. Magnitudes are in AB system using a 5σ limit (see table 3.1).

appears. In the luminosity evolution models considered, the elliptical galaxies are modeled as rapidly fading galaxies at high redshifts, which increases the counts at faint magnitudes. At large distances this population is faint and blue (because the SFR has not decreased that much yet), but as it gets older it brightens (it's also closer to us) and becomes red (the SFR has decreased). The bump at intermediate magnitudes could account for this population. In this type of luminosity evolution galaxies do not disappear, they just age. The fact that the bump is more visible in the I band actually implies that this is the case. Since the faint ellipticals also get redder with age the intermediate bump should be more evident for the I band than for the B band.

The number count models for the I band thus provides an even stronger argument that the luminosity evolution models considered above are just not enough.

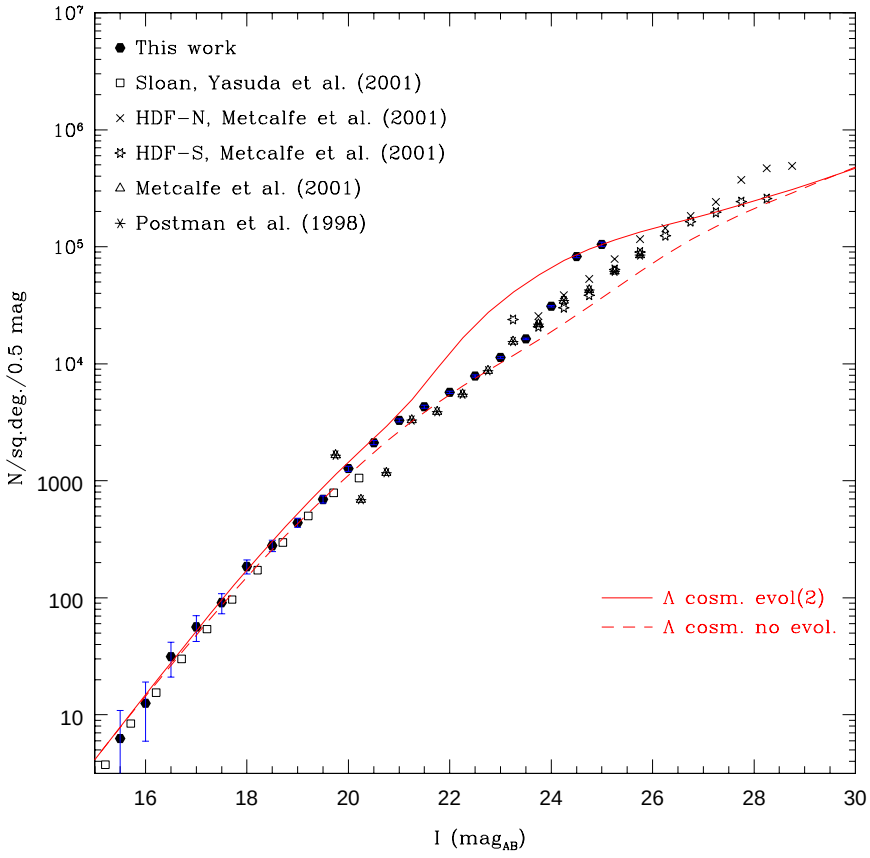

Figure 4.5: Differential number counts in I band with completeness corrections as in table 3.2. Comparison with data from Postman et al. (1998); Metcalfe et al. (2001); Yasuda et al. (2001). **Model number 2** (see chapter 4.1) is used in this plot. Magnitudes are in AB system using a 5σ limit (see table 3.1).

With the inclusion of galaxy merging into the models the faint population would disappear before becoming the relatively bright, redder population which gives rise to the bump. The faint/distant galaxies merge together to form larger galaxies, the total number of galaxies at brighter magnitudes will decrease.

4.4 Comparison with the work of other authors

Metcalfe et al. (2001) have produced number counts from the HDF-N and HDF-S surveys, the data reaches very faint magnitudes. They model galaxy evolution using the same kind of models used in this work but explore more parameters and use a non-Salpeter IMF. They manage to fit the observed numbers counts for bands from U to K over the a range of 10 magnitudes (while having problems with

the brightest and faintest magnitudes). The caveat with their data set is that the HDF's are very small fields, containing on the order of 1000 galaxies, this makes the errors in number counts large and also makes the counts susceptible to systematic errors from angular clustering. The data set used in this work is not as deep as the HDF but contain many more galaxies because of the much larger field of view.

Huang et al. (2001) present number counts of $\sim$4 000 galaxies in B, R and K bands from the Calar Alto Deep Imaging Survey (CADIS) and finds that the observations are best fit by a passive luminosity evolution model. CADIS covers an area roughly the same as the field used in this work (0.2 sq. degrees), but does not go as deep in the optical bands.

Postman et al. (1998) study angular clustering and number counts for a $4^\circ \times 4^\circ$ area containing 710 000 galaxies with $I_{AB} < 24$. They find mild evidence for luminosity evolution of galaxies in their large, but not quite as deep sample.

Yasuda et al. (2001) have produced number counts from the *Sloan Digital Sky Survey* (SDSS) early data release, which is a survey covering a huge part of the sky containing millions of galaxies. Their result give really good counts for brighter magnitudes ($I_{AB} \lesssim 20.5$) which is important for finding the correct normalization for the counts.

5

Galaxy evolution using rest-frame colours and spectral types

5.1 Rest-frame colour evolution for $0.2 < z < 2$

The rest-frame colours for the galaxy sample is binned into redshift bins of 0.2 magnitudes from $z = 0.2$ to $z = 2.0$. The total number of galaxies in each bin decreases with increasing redshift (c.f. figure 3.3), this is due to the fact that the surveyed volume of each redshift bin becomes smaller with increasing redshift, but also due to incompleteness for high redshifts. The adopted magnitude cut at $I \sim 25.17$, limits the amount of faint galaxies found at high redshifts. The errors in the rest-frame colours are quite large (see chapter 3.4), $\delta(U - V) \sim 0.3$ mag., causing the colour distributions to be spread out.

5.1.1 The bimodal distribution of galaxies

Surveys of local galaxies (for example the *Sloan Digital Sky Survey*) show that the galaxy population is divided into two parts (e.g. Hogg et al. 2002). The "red" population has inherently red colours, and thus contain mainly old stars, while the "blue" population has inherently blue colours, containing younger stars and star formation regions. Other authors have found that the bimodality is seen in higher redshift samples as well. For example, Bell et al. (2003) and Im et al. (2002) have found a bimodal distribution up to $z \sim 1$. The rest-frame colour distributions of my data for two colours can be found in figures 5.1, 5.2, 5.3 and 5.4. In the $U - V$ plot I separate the two populations using the same cut as that obtained by Bell et al. (2003). This cut is defined as:

$$< U - V >= 1.18 - 0.38z - 0.08(M_V + 20) \tag{5.1}$$

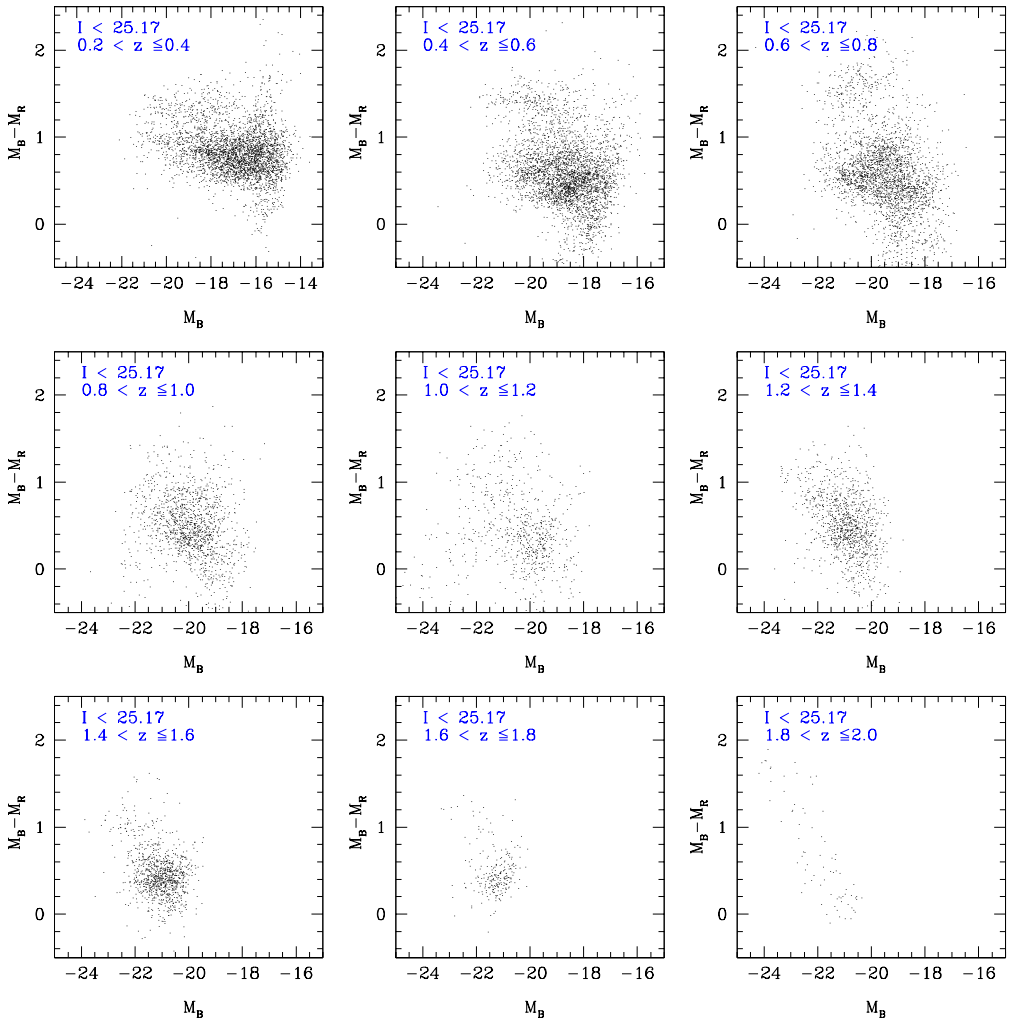

Figure 5.1: Colour distribution for $M_B - M_R$ divided into redshift bins of 0.2 up to $z = 2.0$. The $0 - 0.2$ bin is excluded because of large photometric redshift uncertainties. Bright blue galaxies (see text) are clearly absent from the low-z bins, but present in the high-z ones.

Galaxies above this cut are considered to be part of the red population. The distribution of galaxies is clearly bimodal up to $z \sim 1.5$. Even for the higher redshifts there is a small "red" peak in the colour distribution, but the few numbers of galaxies makes the relative errors grow too large to really say if this is a significant effect.

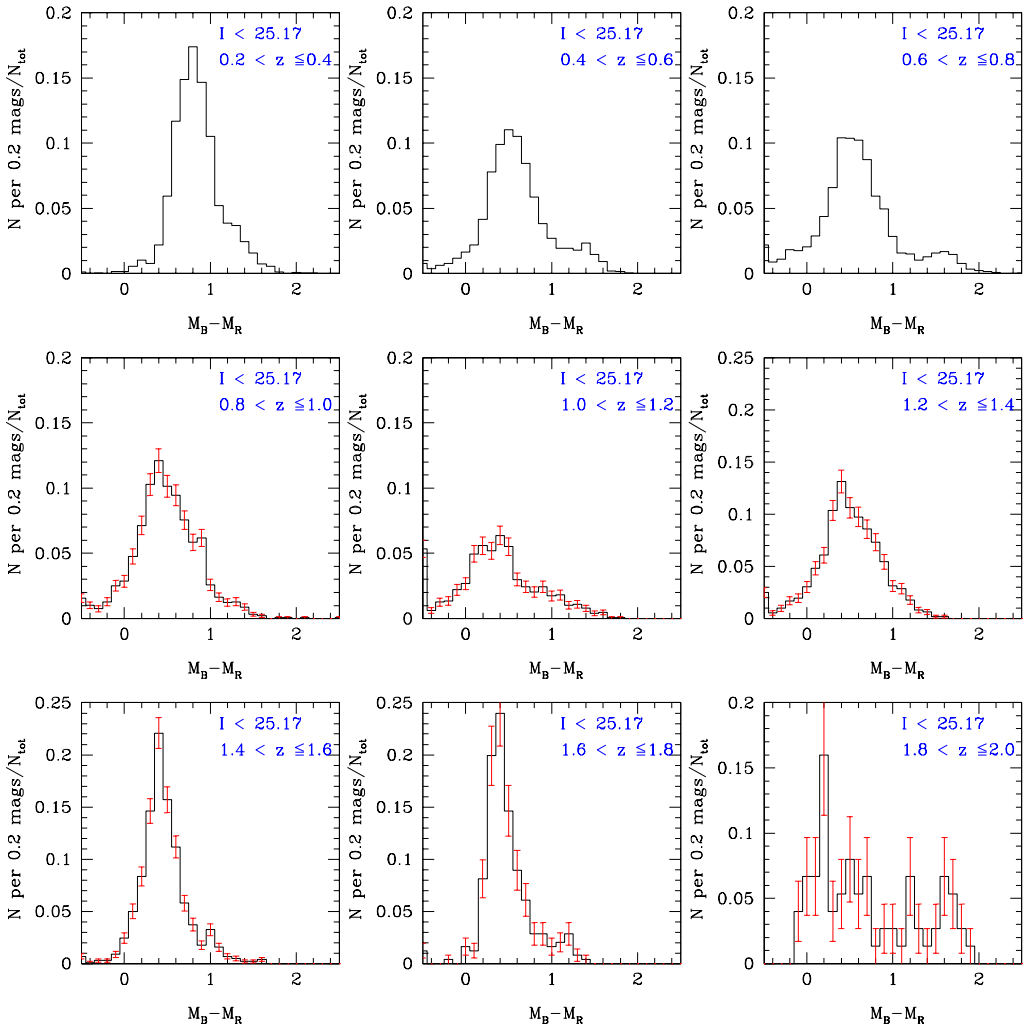

Figure 5.2: Colour distribution histograms for $M_B - M_R$ divided into redshift bins of 0.2 up to $z = 2.0$. The $0 - 0.2$ bin is excluded because of large photometric redshift uncertainties. The bimodal distribution of galaxies (see text) is clearly visible up to $z \sim 1.0$. Error bars for $z > 0.8$ are estimated as Poisson errors. N_{tot} is the total number of galaxies in the redshift bin under consideration.

5.1.2 Evolution of the "red" galaxy population

Bell et al. (2003) claim that the red population is reddened by ~ 0.4 magnitudes when going from $z \sim 1$ to $z \sim 0.2$. This effect can be seen in figures 5.2 and 5.4. It is most easily seen in the $U - V$ plot, the reason for this being that the rest-

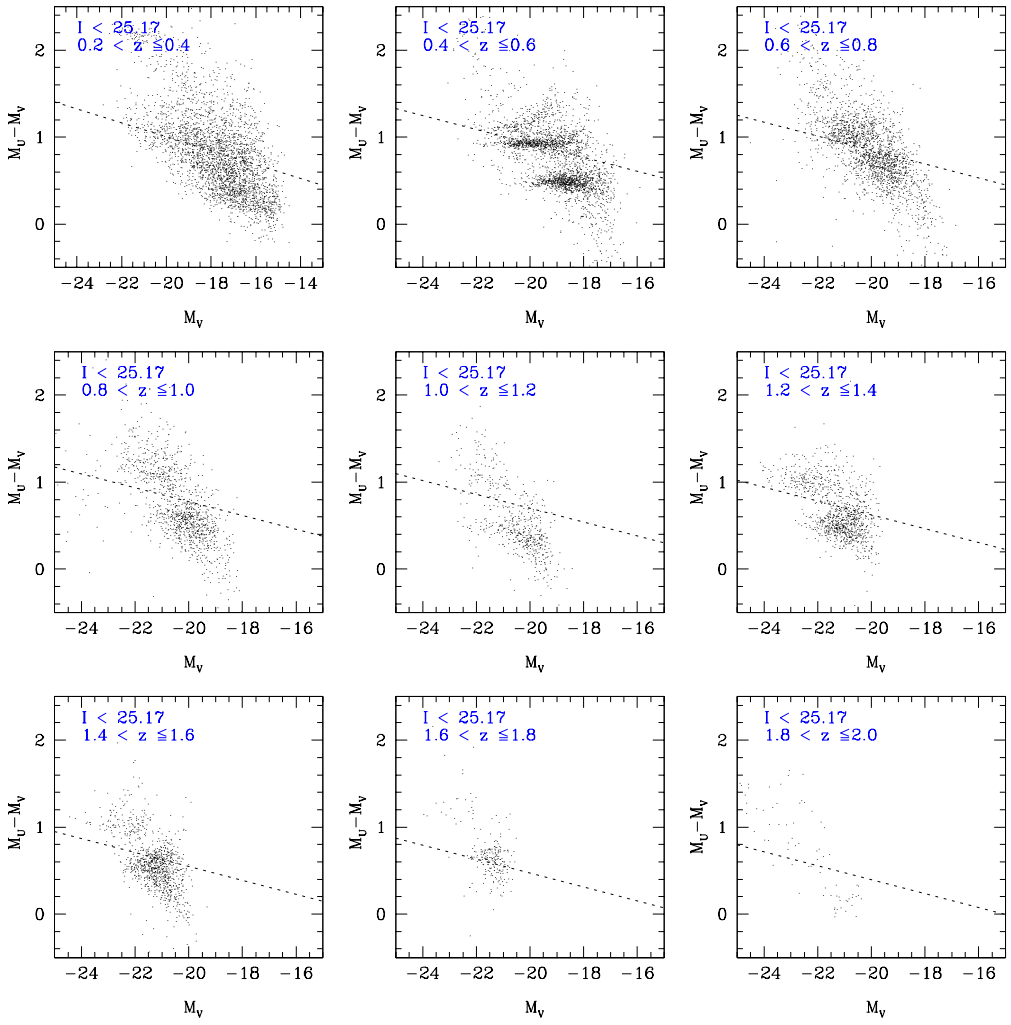

Figure 5.3: Colour distribution for $M_U - M_V$ divided into redshift bins of 0.2 up to $z = 2.0$. The $0 - 0.2$ bin is excluded because of large photometric redshift uncertainties. Bright blue galaxies (see text) are clearly absent from the low-z bins, but present in the high-z ones.

frame $U - V$ colour efficiently traces star forming galaxies, so that when a galaxy stops forming stars it joins the red population. The rest colour evolution from $z \sim 1.3$ to $z \sim 0.3$ for $U - V$ is shown in figure 5.5. The observed reddening is ~ 0.5 magnitudes, and the relation seem to flatten out at $z > 1$. The observed data points are computed as the mean colours of objects in the considered redshift bin and that belong to the red population (defined by the cut, see text above).

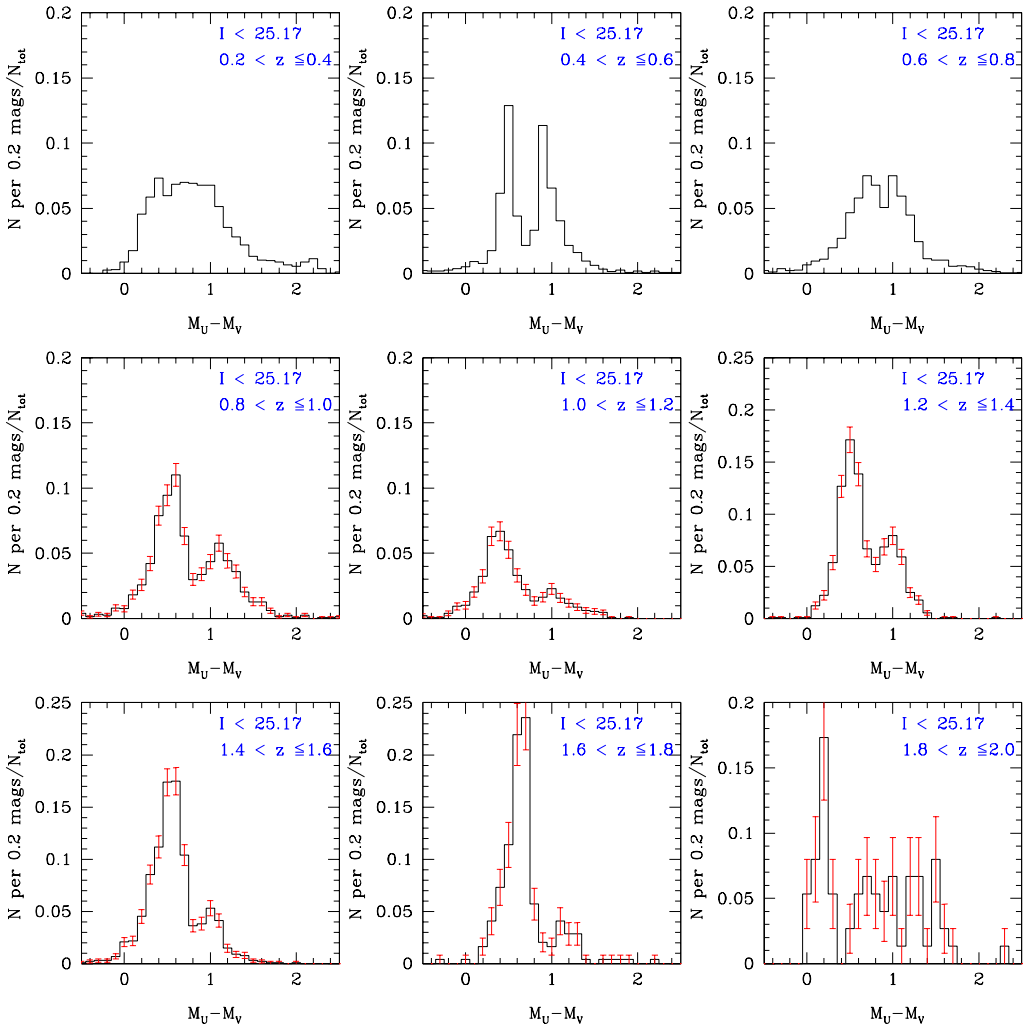

Figure 5.4: Colour distribution histograms for $M_U - M_V$ divided into redshift bins of 0.2 up to $z = 2.0$. The $0 - 0.2$ bin is excluded because of large photometric redshift uncertainties. The bimodal distribution of galaxies (see text) is clearly visible up to z 1.5. Error bars for $z > 0.8$ are estimated as Poisson errors. N_{tot} is the total number of galaxies in the redshift bin under consideration.

However, the effect of outliers (i.e. galaxies that cannot be defined by a simple colour-magnitude relation) can be significant when computing mean values. This especially applies to the two last data points where it is difficult to find a simple colour-magnitude relation. The flattening of the colour evolution at redshifts above

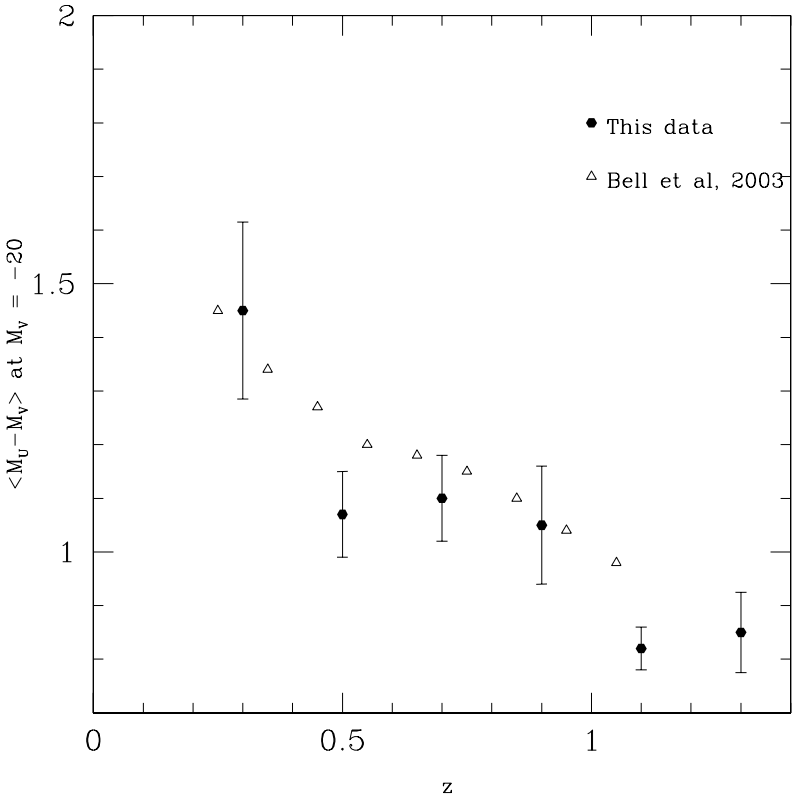

Figure 5.5: Color evolution of the "red population" at magnitude $M_V = 20$ (using a binsize of 0.5 magnitudes). Error bars show the 1σ scatter around the mean. Open triangles show the data of Bell et al. (2003).

1 is therefore highly uncertain. However, if true, it might indicate when the very first galaxies was formed. Bell et al. (2003) has compared their observed colour evolution to models of single-age stellar populations formed at different redshifts and at different metallicities. Comparing with their models a tentative conclusion is that the the formation redshift of the red population is most probably > 5.

5.1.3 Evolution of the "blue" galaxy population

The blue population does not seem to change with increasing redshift if we look at the median colours (i.e. the peaks in the colour histograms figures 5.2 and 5.4). The evolution of the blue galaxies is fundamentally different from the evolution of the red galaxies. Instead of a colour evolution where the galaxies grow bluer and bluer for increasing redshift, it is the number density of blue galaxies that evolve. The relative number (compared to the total number of galaxies in the chosen redshift bin) of all blue galaxies increases with higher redshift (c.f. Lilly et al. 1995b; Bell

et al. 2003). The luminous blue galaxies become *much* more common at higher redshift. For the lowest redshift bin ($z \sim 0.3$) there are almost no blue galaxies brighter than $M_V = -23$. The numbers of bright blue galaxies then increases for higher and higher redshifts up to $z \sim 1.5$. For $z > 1.6$ there is a sharp decline, it is hard to say where this comes from. It might be a dusty environment that causes the bright blue galaxies to fade, this is also supported by the fact that there seems to exist "red" galaxies at these high redshifts. One should, however bear in mind that at $z \sim 1.6$ we are getting close to the limit of the sample. Redshift incompleteness will most probably affect the counts, an extensive analysis of the incompleteness due to magnitude and redshift divided into galaxy types (e.g. Wolf et al. 2003) is needed to find out if this is a "real" effect.

Butcher & Oemler (1984) studied 33 galaxy clusters ($0.003 < z < 0.54$) and found that the fraction, f_B, increased with redshift, this is therefore called the *Butcher-Oemler effect*. Since their discovery many other authors have studied this effect in observations of intermediate redshift clusters (e.g. van Dokkum et al. 2000; Dahlén, Fransson & Näslund 2002). The problem with going to clusters at higher redshifts is that the contamination from field galaxies becomes too large at high redshifts. Diaferio et al. (2001) have used hierarchical clustering models to study the Butcher-Oemler effect in a λCDM universe and found good agreement between the models and observations. They also found that f_B increases with redshift also for field galaxies, but were unable to model the rapid increase found in surveys (e.g. CNOC1, Yee, Ellingson, & Carlberg 1996). Since f_B is used as property for a galaxy cluster it is normally defined as the fraction of galaxies with $M_V < -20$, inside a certain radius, that are 0.2 magnitudes bluer than the colours of early type galaxies.

In figure 5.6 the fraction of blue galaxies versus redshift for the field galaxies in this data set is plotted. Here f_B is defined as the fraction of galaxies bluer than the colour cut in equation 5.1 for galaxies brighter than $M_V = -20$. The fraction was computed for each of the redshift bins after making the magnitude cut. The plot clearly shows that the conclusions drawn from quantitatively inspecting the colour distribution plots are correct. The fraction of bright blue galaxies increase with redshift up to $z \sim 1.5$, the evolution in f_B is very strong, going from ~ 0.1 for the lowest redshift bin up to ~ 0.8 for $z \sim 1.5$. The estimated errors are quite large (due to the large uncertainties in the rest frame colours) but the trend is clearly visible. For $z \gtrsim 1.5$, f_B stops increasing and starts decreasing instead. Due to the previously mentioned problems with redshift incompleteness it is hard to say if the fraction is leveling out or if it really starts to decrease.

The faint blue galaxies seem to be as common at low redshifts as at high for the redshift range $0.3 \lesssim z \lesssim 1.0$ (where I consider galaxies in the blue population with $M_V > -20$ to be faint). For higher redshift it becomes hard to say what happens to this population due to incompleteness.

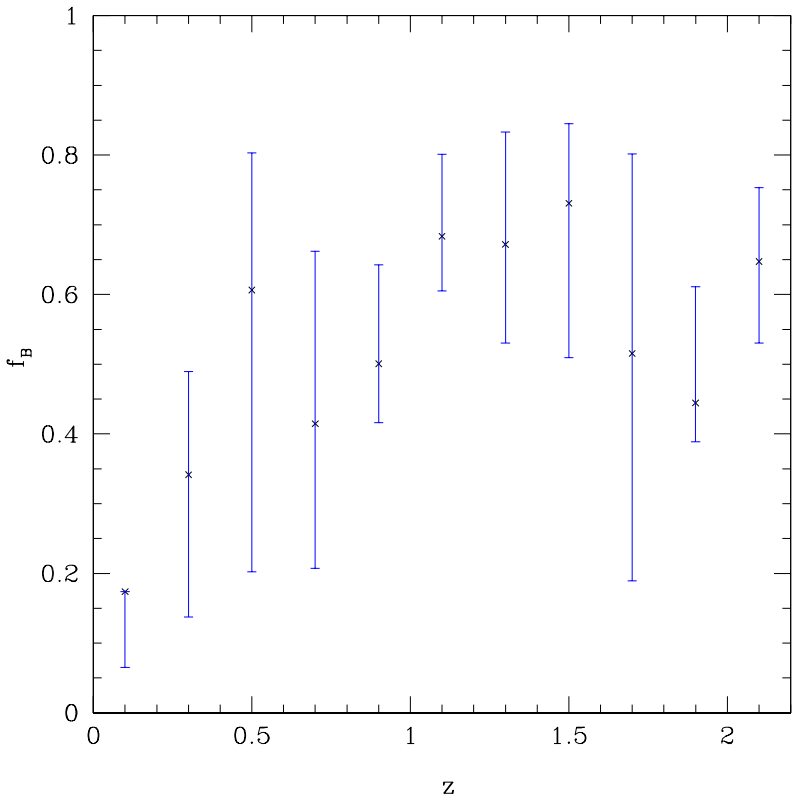

Figure 5.6: The fraction of galaxies with $M_V < -20$ which are considered to be blue, i.e. has a $U - V$ colour smaller than the cut defined in equation 5.1. Errorbars mark the low and high values obtained by scattering the magnitudes by the rms error of the absolute magnitudes ($\delta(U - V) \sim 0.3$ mag.).

5.2 Spectral type evolution for $0.2 < z < 2$

The distribution of galaxies binned in galaxy type and redshift is shown in figure 5.7. The main result is that late-type galaxies are much more common at high than at low redshift, this is also consistent with the results from the rest-frame colour distributions. At low redshifts (up to $z \sim 0.5$) starburst galaxies are almost nonexistent. At redshifts $\gtrsim 0.5$ the numbers of type 4-6 (Irr, SB2, SB3) starts to increase and in the highest redshift bins they are the most common type.

The spectral type of galaxies is closely related to the morphology of galaxies. The spectral types used (Coleman, Weedman &Wu 1980) are obtained as the mean of spectra from galaxies of the different morphological types. For ground-based observations the best way to determine the morphology of high-z galaxies is to find the spectral type via template fitting. Space-based observations with superior resolution show how well SED fitting correlates with morphology (Wiegert 2003).

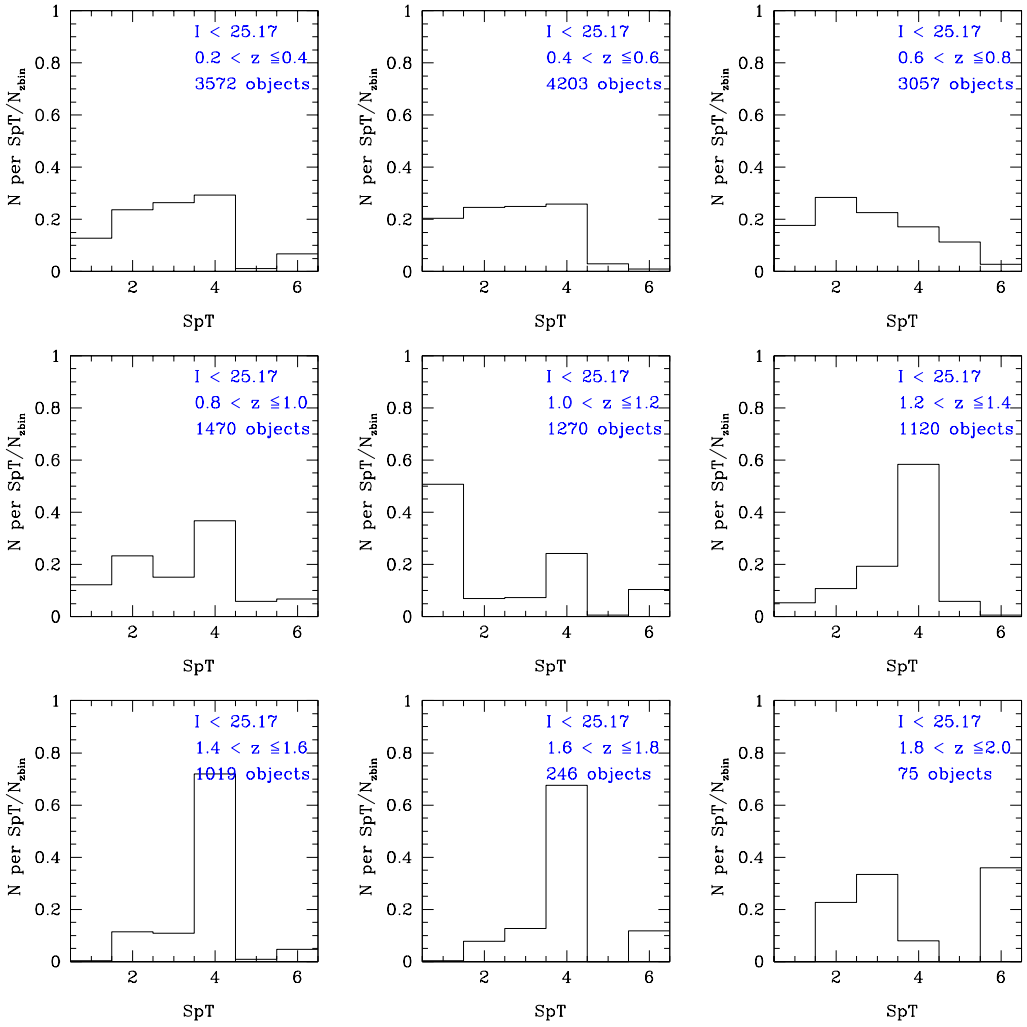

Figure 5.7: Numbers of galaxies identified as a specific spectral type, 1) E/S0, 2) Sbc, 3) Scd, 4) Irr, 5) SB2, 6) SB3. The galaxy classification is made by BPZ using the templates from Coleman, Weedman &Wu (1980); Kinney et al. (1996). Numbers have been normalized by dividing by the total number of galaxies in each redshift bin (N_{zbin}). The numbers of irregular and starburst galaxies clearly grows with increasing redshift.

Abraham et al. (1996) found rapidly increasing number counts for the irr/pec class of galaxies in HDF-N, this is consistent with a higher fraction of type 4-6 galaxies at high redshifts. In this thesis we use observations of a field which is much larger than the HDF, this means that the observed numbers of galaxies are much larger

and therefore also that the errors are smaller. Hierarchical clustering theory also predict high fractions of irregular (merging) systems at high redshift (Cole et al. 2000).

The numbers of late type galaxies does not change for redshifts $\lesssim 1$ but then start to decrease, with the notable exception of ellipticals in the $z \sim 1.1$ bin. In this bin a lot of elliptical galaxies are found, the reason for this is most probably problems with the photometric redshifts where faint ellipticals at a lower redshifts are wrongly placed in this bin. It could also be a sign of a cluster in the field at $z \sim 1$ but the ellipticals in this bin are not related spatially which rules out this theory.

The fact that I investigate two properties of the galaxy population (type and redshift), which were both obtained as the best-fit parameters in a maximum-likelihood type method could in principle add systematic effects to the distributions. Since the studied filter set is limited (a given type-redshift combination might not be detected in the chosen filter set) there might be a bias in the method. To investigate this bias the incompleteness functions for the different galaxy types, magnitudes and redshifts need to be included in the analysis.

6

Conclusions

6.1 Summary and discussion

This work has investigated observational clues to how galaxies form and evolve. By using multicolor observations in both optical and near-IR bands I have been able to find photometric redshifts for 21 053 galaxies. In the range $0.2 < z \lesssim 2.3$ the rms dispersion of the photometric redshifts (when compared to the spectroscopic redshifts of 223 sources) is found to be $0.13(1+z)$. The amount of galaxies with very large errors ($\Delta z > 1$) in the redshift estimation is also quite small in this range ($\lesssim 4\%$). The galaxy sample was then divided into redshift bins, and the rest-frame colour evolution of the total population could be studied. The size of the data sample is among the largest studied so far, comparable to the COMBO-17 survey (Wolf et al. 2003) in size and redshift range. The main conclusions of the analysis are:

- The redshift distribution of galaxies does not contain any obvious peaks, which suggest that CDF-S is devoid of any large galaxy clusters. This is also confirmed when studying the rest-frame colours of the sample.

- Very faint galaxies which lack U band photometry are often misclassified as starburst galaxies with high redshifts by BPZ. There seem to be a bias toward choosing the starburst template as the best fit when the photometry is bad or lacking in several bands. The fact that very highly redshifted galaxies are expected to lack U band (so called U-dropouts) cannot be the reason for the large amount of galaxies placed at redshift 3-4. By improving the photometry (or making a more conservative magnitude cut) this effect can be countered.

- The completeness corrected number counts of the galaxy sample have been compared to two luminosity evolution models and one non-evolution model,

all three using a standard λCDM cosmology. It is found that the non-evolution model fit the data well at bright magnitudes, but underpredict the number of faint galaxies (i.e. the faint blue galaxy problem discussed by e.g. Ellis 2001). The use of λCDM cosmology gives all of the models a "boost" in numbers of faint galaxies, as compared to the earlier non-λ cosmology. This effect is, however, not enough. I have also tried to include luminosity evolution into the models. The luminosity evolution models fit the data better at the faint end, but have problems with the intermediate range. The best models still need to be modified to fit the observations, probably by including hierarchical clustering and dust extinction.

- The numbers of bright blue galaxies is much higher at high redshifts than at low. This has also been found by many other authors (Lilly et al. 1995b; Lin et al. 1999; Wolf et al. 2003; Bell et al. 2003). The fraction of blue galaxies among galaxies brighter than $M_V = -20$ increases from ~ 0.1 to ~ 0.7 over the redshift range 0.1-1.3. For $z \gtrsim 1.3$ the fraction seems to be decreasing, but redshift incompleteness and selection effects become more and more important for higher redshifts so these results are somewhat uncertain. The numbers of faint blue galaxies (where faint means galaxies with $M_V > -20$) does not seem to change over the redshift interval $0.2 < z \lesssim 1.5$.

- The red galaxy population is well characterized by a colour-magnitude relation with the same slope at all redshift bins in the range $0.2 < z \lesssim 1.1$, for the $z \sim 1.3$ bin the relation is unclear. The mean colour of the population do however evolve with redshift. From $z \sim 0.3$ to $z \sim 1.3$ the red galaxy population is reddened by 0.5 magnitudes. The colour evolution with redshift seem to flatten out at redshifts $\gtrsim 1.2$ but this is uncertain due to the problems with the colour-magnitude relation at such high redshifts.

- Late type galaxies are more common at higher redshifts. Starburst and irregular galaxies become more and more common as we go back in time. Starting at $z \sim 0.5$ the fractions of these galaxy types increase and for the highest redshift bins in the sample they are the most common type. It is hard to tell if the numbers of early type galaxies change significantly over the redshift range under consideration ($0.2 < z \lesssim 2$), it seems to be fairly constant up to $z \sim 1.3$. Thereafter the numbers drop but due to the small total number of galaxies in these bins it is hard to know whether this drop is real.

Taken together the conclusions can give us a schematic of how galaxies are formed and evolve. The fact that many more faint galaxies are found than what would be expected points us in the direction of raising the total number of primordial galaxies and accepting that galaxy merging is a very common event in the universe. The first building blocks of todays galaxies might have been small dwarfs at very high redshifts (at $z > 5$), the red population at high redshifts could

in fact then be 2nd or 3rd generation mergers which at redshifts < 2 would have aged to the observed red colours. At each merger, star formation could have been triggered anew, the bigger the participating galaxies the more luminous merging system (with more star formation). The red population thus traces galaxies which have not undergone a major merger for a long time. The bright blue galaxies at intermediate redshift is then the result of merging by even later generations of galaxies. Since the supply of galaxies is not unlimited the merging of galaxies is expected to start decreasing at some redshift, which would result in fewer bright blues at low redshifts. We would expect to see some kind of peak in the fraction of bright blue galaxies at some intermediate redshift since the amount of large mergers is expected to grow bigger and bigger until the above limit is reached.

6.2 Future work

The rest-frame colour evolution has provided us with some clues to how galaxies form and evolve, but there are other methods which can be used. Wolf et al. (2003); Chen et al. (2003) among many others have studied evolution of the luminosity function, binned into different spectral types. The distribution of galaxy types and their evolution can be modeled in theory and the parameters of the luminosity function used (Φ^* and M^*) can be compared to the best-fit parameters from the observations. In this way the luminosity and galaxy evolution can be studied in greater detail, for example merger rates of galaxies can be determined. Constructing luminosity functions of the redshift/type binned data and find the best-fit parameters is therefore an important task for the future. The luminosity functions of field and cluster galaxies has been found to be different (Binggeli, Sandage & Tammann 1988), it would be interesting to compare the found functions to studies of galaxy clusters (e.g. Dahlén, Fransson & Näslund 2002; Chen et al. 2003).

The number count models used does clearly not fit the observations over the full magnitude range. Models including dust and/or hierarchical clustering would be very interesting to compare with.

The angular correlation function is used as a measure on how "clustered" galaxies are, do most galaxies appear in pairs or groups, and does this change with redshift? The clustering statistics can be used to check the theories of galaxy formation and evolution, but also evolution and formation of the larger scale structures might be studied. Using the photometric redshifts of the sample galaxies we can study the evolution of the angular correlation function with redshift.

The total sample of 21 053 galaxies can be studied further by choosing a certain part of the redshift and luminosity range, for example the very red (i.e. rest-frame) galaxies at $z > 2$. Why are these galaxies so red, is it that they are old galaxies already at $z \sim 2$, or are they younger galaxies within a very dusty environment? This population might be interesting to study in further observations, perhaps going to sub-mm wavelengths to probe their true nature.

References

Abraham R. G., Tanvir N. R., Santiago B. X., Ellis R. S., Glazebrook K., van den Bergh S. 1996, MNRAS, 279, L47

Arnouts S., D'Odorico, S., Cristiani, S., Zaggia, S., Fontana, S., Giallongo, S. 1999, A&A, 341, 641

Arnouts S. et al. 2001, A&A, 379, 740

Bell, E. F., Wolf, C., Mesienheimer, K., Rix, H. W., Borch, A, Dye, S, Kleinheinrich, M., McIntosh, D. H. 2003, astro-ph/0303394, submitted to ApJ

Benítez, N. 2000, ApJ, 536, 571

Bershady, M.A., Lowenthal, J.D., Koo, D.C. 1998, ApJ, 505, 50

Bertin, E., Arnouts, S. 1996, A&AS, 117, 393

Binggeli, B., Sandage, A., Tammann, G. A. 1988, ARA&A, 26, 509

Bolzonella, M., Miralles J.-M., Pelló R. 2000, A&A, 363, 476

Bruzual, G., Charlot, S. 1993, ApJ, 405, 538

Butcher H., Oemler A. 1984, ApJ, 285, 426

Campos, A. 1995, astro-ph/9510051

Chen, H. et al. 2003, ApJ, 586, 745

Cole, S., Lacey, C. G., Baugh, C. M., Frenk, C. S. 2000, MNRAS, 319, 168

Coleman G. D., Wu C.-C., Weedman D. W. 1980, ApJS, 43, 393

Connolly, A. J., Szalay, A. S., Koo, D. C., Kron, R. G., Munn, J. A. 1995, AJ, 110, 2655

Crampton, D., Le Fevre, O., Lilly, S. J., Hammer, F. 1995, ApJ, 455, 96

Dahlén, T. 2002, Ph. D. thesis, Stockholm University

Dahlén, T., Fransson, C., Näslund, M. 2002, MNRAS, 330, 167

Diaferio, D., Kauffmann, G., Balogh, M., L., White, S., D., M., Schade, D., Ellingson, E. 2001, MNRAS, 323, 999

Ellis, R. S. 2001, astro-ph/0102056

Fernández-Soto, A., Lanzetta, K.M., Yahil, A. 1999, AJ, 513, 34

Gardner, J. P., Sharples, R. M., Carrasco, B. E., Frenk, C. S. 1996, MNRAS, 282, L1

Gwyn, S. 1995, MS Thesis, University of Victoria

Hogg, D. W., et al. 2002, AJ, 124, 646

Hogg, D. W., Baldry, I. K., Blanton, M. R., Eisenstein D. J. 2002, astro-ph/0210394

Huang, J.-S. et al. 2001, A&A, 368, 787

Im, M., et al. 2002, ApJ, 571, 1361

Kinney, A. L., Calzetti, D., Bohlin, R. C., McQuade, K., Storchi-Bergmann, T., Schmitt, H. R. 1996, ApJ, 467, 38

Kron, R. G. 1980, ApJS, 43, 305

Lilly, S. J., Le Fevre, O., Crampton, D., Hammer, F., Tresse, L. 1995a, ApJ, 455, 50

Lilly, S. J., Le Fevre, O., Crampton, D., Hammer, F., Tresse, L. 1995b, ApJ, 455, 108

Lin, H. et al. 1999, ApJ, 518, 533

Longair, M.S. 1998, *Galaxy Formation*, Springer-Verlag

Madau P. 1995, ApJ, 441, 18

Metcalfe N., Shanks T., Campos A, McCracken H.J., Fong R. 2001, MNRAS, 323, 795

Minezaki, T., Kobayashi, Y., Yoshii, Y., Peterson, B.A. 1998, ApJ, 494, 111

Nagashima, M., Yoshii, Y., Totani, T., Gouda, N. 2002, ApJ, 578, 675

Nakata, N. et al. 1999, MNRAS, 309, L25

Oke, J. B., Gunn, J. E. 1983, ApJ, 266, 713

Peebles, P. J. E. 1983, ApJ, 263, L1

Peebles, P. J. E. 1998, *Principles of Physical Cosmology*, Princeton University Press

Postman, M., Lauer, T. R., Szapudi, I., Oegerle, W. 1998, ApJ, 506, 33

Press, W. H., Schechter, P. 1974, ApJ, 187, 425

van Dokkum P. G., Franx M., Fabricant D., Illingworth G. D., Kelson D. D. 2000, ApJ, 541, 95

Vandame, B. et al. 2001, astro-ph/0102300, submitted to A&A

Wiegert, T. 2003, MS thesis, Chalmers University of Technology

Williams, R. E. et al. 1996, AJ, 112, 1335

Wolf, C., Meisenheimer, K., Rix, H.-W., Borch, A., Dye, S., Kleinheinrich, M. 2003, A&A, 401, 73

Salpeter, E. E. 1955, ApJ, 121, 161

Saracco, P., D'Odorico, S., Moorwood, A., Buzzoni, A., Cuby, J.-G., Lidman, C. 1999, A&A, 349, 751

Shanks T., Stevenson P. R. F., Fong R., MacGillivray H. T. 1984, MNRAS, 206, 767

Sterken, Chr., Manfroid, J. 1992, *Astronomical Photometry*, Kluwer Academic Publishers

Yan, L., McArthy, P.J., Storri-Lombardi, L.J., Weymann, R.J. 1998, ApJ, 503, L19

Yasuda N. et al. 2001, AJ, 122, 1104

Yee H. K. C., Ellingson E., Carlberg R. G., 1996, ApJS, 102, 269

Zeldovich, Ya. B. 1993, In *Selected works of Yakov Borisevich Zeldovich, Vol. 2, Particles, Nuclei and the Universe*, (eds. J. P. Ohstriker, G. I. Barenblatt & R. A. Sunyaev), Princeton University Press